C.P. No. 598

MINISTRY OF AVIATION

AERONAUTICAL RESEARCH COUNCIL

CURRENT PAPERS

The Effect of Tip Bluntness on Boundary-Layer Transition on a 15° Included Angle Cone at M = 3.12 and 3.81

by

Ruth H. Rogers

LONDON: HER MAJESTY'S STATIONERY OFFICE

1962

SIX SHILLINGS NET

ADDENDUM

In the calculation of the theoretical curves in Fig.15, the value of ν_o in the formula used (equation (2) of Appendix 1) was taken to be the value in the free stream. This is incorrect, because ν_o is a function of the local stagnation pressure at the edge of the boundary layer, and this varies with x/r. The calculations have been repeated using the true value of ν_o, and the curve replotted in the attached figure. It is seen that the experimental points are in fair agreement with this curve.

As pointed out in the introduction to the main text, the above formula is derived by Rott and Crabtree[2] for a stream in which the pressure gradient is a function of x, but whose velocity in the external flow is independent of z. In the present case, neither of these conditions hold, and the variation with x of the Mach number, M, at the edge of the boundary layer is caused by the variation of local stagnation pressure with x. It is reasonable to suppose, however, that the cause of the variation of M, with x does not greatly affect the development of the boundary layer; therefore the formula should give a good approximation for this problem.

Calculations of the quantity $R_{\delta_2}/\sqrt{rp_o}$, as discussed in section 4.5 have been carried out, and the quantity $m + \frac{1}{2} n$ defined in that section has been calculated. The accuracy of the calculations is dependent on the experimental variation of M_1 with x/r, and is therefore limited. The accuracy is insufficient to determine whether $m + \frac{1}{2} n$ is greater or less than 1/2 in the neighbourhood of x = 100 r, and the calculations show merely that $m + \frac{1}{2} n$ is near 1/2. The arguments of section 4.5, therefore, are still inconclusive; it seems certain, however, that if R_{δ_2} is a more appropriate parameter than R_x to determine the position of transition, $x = x_t$, the variation of δ_2 with x is just as important as the variation of the Reynolds number per inch, which was assumed by Moeckel[1] to be the sole criterion. It seems, therefore, that the sign of the quantity dx_t/dr is less easily predicted than was previously supposed; in fact, it may be very sensitive to small irregularities in the stream or on the surface of the model.

FIG. 15. (a & b) REVISED.

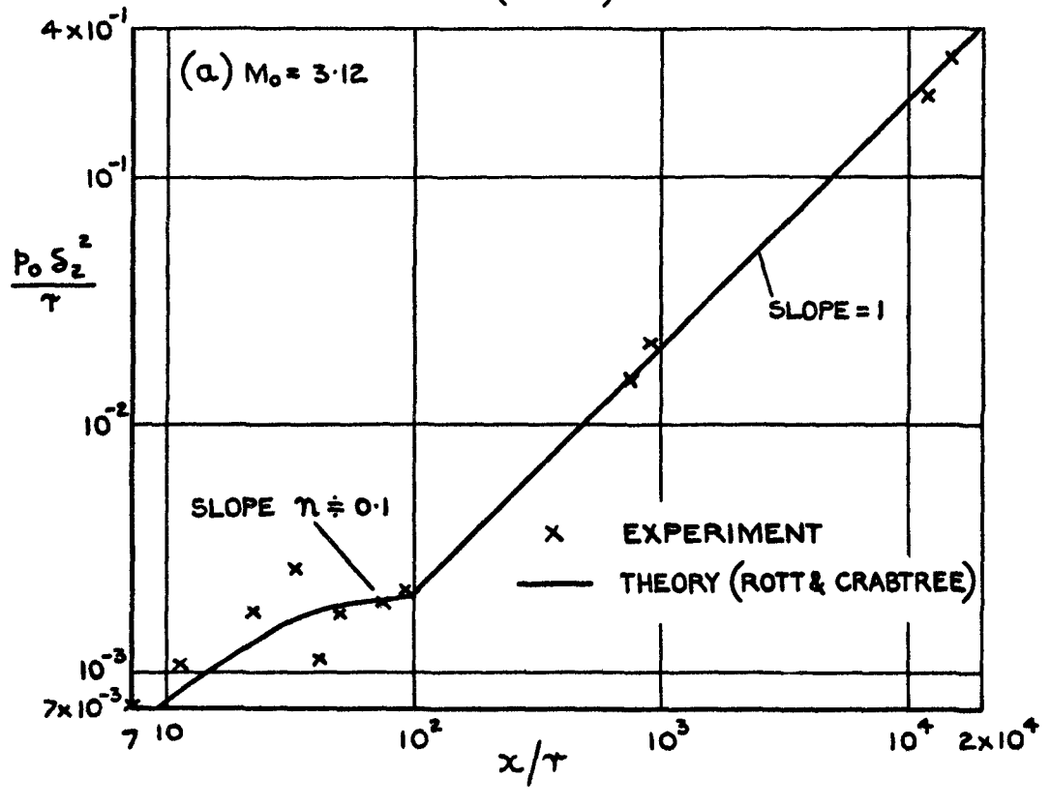

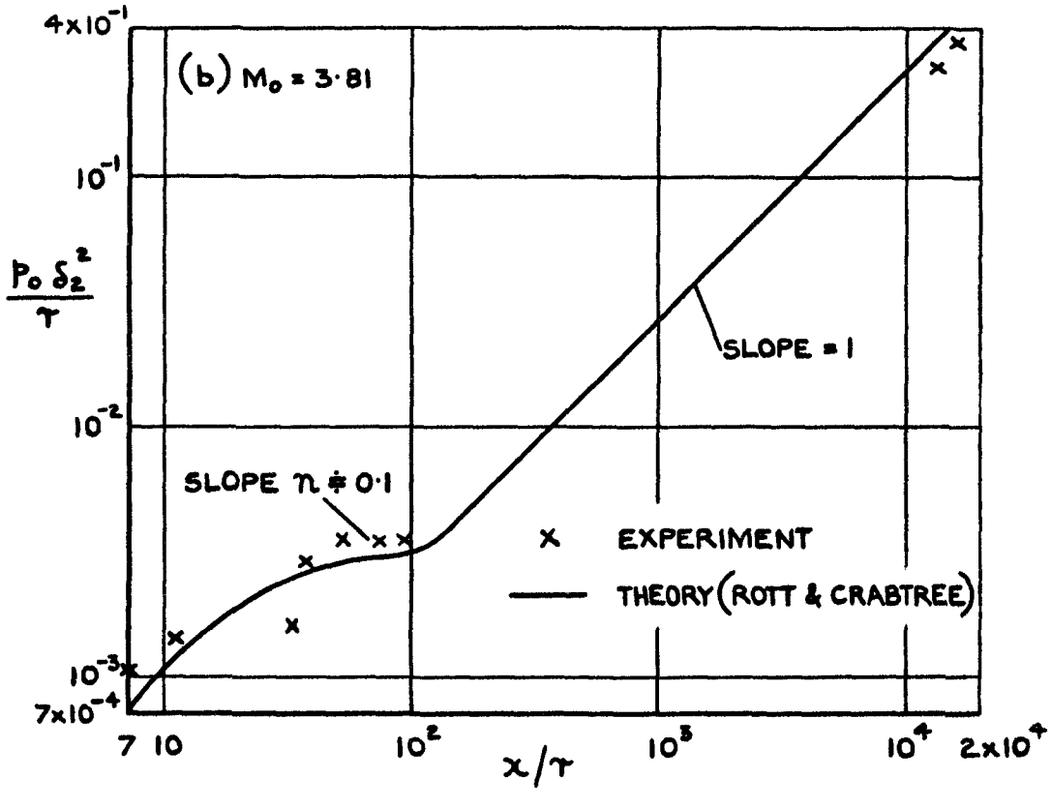

VARIATION OF $\rho_0 \delta_2^2 / \tau$ WITH x/τ
(a). $M_0 = 3{\cdot}12$, (b). $M_0 = 3{\cdot}81$.

U.D.C. No. 533.6.011.5:532.526.3:533.696.4

C.P. No. 598

August, 1959

THE EFFECT OF TIP BLUNTNESS ON BOUNDARY-LAYER TRANSITION ON A 15° INCLUDED ANGLE CONE AT M = 3.12 AND 3.81

by

Ruth H. Rogers

SUMMARY

Cones having a 15° included angle and tip-radii up to 0.49" were tested at free stream Mach numbers of 3.12 and 3.81 at zero incidence. The position of transition to turbulence in the boundary layer was found to move downstream as tip radius increased, as long as transition was more than about 100 tip radii downstream from the tip. If transition occurred upstream of this station, its position tended to move further upstream as tip radius increased. Pitot traverses of the boundary layer were made, and showed that the Reynolds number based on momentum thickness at transition remained nearly constant in all cases (at 680 when M = 3.12 and 600 when M = 3.81). Some tentative arguments are put forward to explain the upstream movement of transition when occurring near the tip.

Previously issued as R.A.E. Tech Note No. Aero 2645 - A.R.C. 21,695.

LIST OF CONTENTS

LIST OF APPENDICES

LIST OF TABLES

LIST OF ILLUSTRATIONS

1 INTRODUCTION

When a smooth cone with a sharp tip is placed at zero incidence in a uniform supersonic air stream, there is an attached conical shock. A laminar boundary layer develops on the surface of the cone; the conditions at the edge of the boundary are essentially uniform over the whole cone.

If a blunt cone is placed in the same air stream, there is a detached bow shock, which develops into a conical shock further downstream. The conditions at the edge of the boundary layer are no longer uniform over the whole surface, for near the tip the fluid has passed through a nearly normal shock wave but far from the tip, the fluid has passed through a nearly conical shock (see Fig.1 and note Fig.12 which shows local Mach numbers obtained in the present tests). It is to be expected, therefore, that the position of transition to turbulence is different from that on a sharp cone.

Moeckel[1] has pointed out that the Reynolds number per inch, $\rho u/\mu$, based on conditions at the edge of the boundary layer, will increase with distance, x, from the tip up to the value $\rho_\infty u_\infty/\mu_\infty$ corresponding to a sharp cone. This agrees with the present test results, note Fig.13. Therefore, if transition occurs at a given value of $R_x = \rho u\, x_t/\mu$, the value of x_t will be larger on a blunt nosed cone than on a sharp cone. The present tests were designed to check this, and to determine the order of magnitude of the effect.

It was found that transition on a blunt cone occurred for a larger value of x than on the corresponding sharp cone in the same stream as long as x_t was greater than 100 r, where r is the radius of the tip. For x_t less than 100 r, the trend was reversed (at least for x_t greater than about 80 r). The values of Reynolds number per inch ($\rho u/\mu$) at the edge of the boundary layer were measured (see Fig.13), and it was found that $\rho u/\mu$ increased rapidly with x for x less than 100 r, and had reached the sharp cone value $\rho_\infty u_\infty/\mu_\infty$ for x greater than 1,000 r. It is therefore a little surprising that the effect predicted by Moeckel should be found in the region $x_t > 100$ r; maybe the previous history of the boundary layer is of importance.

However, it was more surprising that in the region where Moeckel's argument would be expected to hold (x less than 100 r) the reverse effect was observed. Traverses of the boundary layer showed that, for a wide range of values of x/r, the value of R_{δ_2} at transition did not vary much from 680 at $M_o = 3.12$ and 600 at $M_o = 3.81$. This suggests that the instability which causes transition to turbulence is of the same nature as that for a sharp cone. Measured values of the momentum thickness in this region were, however, larger than would be expected on sharp-cone theory (see Fig.15), and larger still than would be given by a theory allowing for the measured variation of Mach number at the outer edge of the boundary layer. This enhancement of momentum thickness counterbalances the reduction in Reynolds number per inch and leads to the reversed trend observed in the region $80 < x/r < 100$.

The theoretical values of δ_2 were obtained from Rott and Crabtree's formula[2]

$$\delta_2^2 = 0.45\, \nu_o \left(\frac{T_1}{T_o}\right)^{-3} u_1^{-6}\, r_o^{-2} \int_o^s \left(\frac{T_1}{T_o}\right)^{1.5} u_1^5\, r_o^2\, ds$$

using the measured values of M_1 (Fig.12). The resulting curve is shown in Fig.15, and gives smaller values than for a sharp cone instead of the measured larger ones. The reason for the discrepancy may be that in its derivation the formula includes the usual assumption that, outside the boundary layer, the velocity does not vary with distance from the surface. However, there is a region for $x < 100\ r$ where there is a pronounced variation of this nature (see the pitot pressure results for intermediate x/r in Figs. 10 and 11), so that the above formula would not be applicable.

The development of the boundary layer in an external shear flow has been discussed by Li[3,4], Yen[5], Glauert[6] and Murray[7], and it may be that an extension of their work is applicable here, (but such an extension was considered to be beyond the scope of the present note).

It is worth noting that a simple Mangler transformation yields a ratio, $\left(\int r_o^2\, dx\right) / r_o^2\, x$, which differs significantly from its value on a sharp cone only when x is less than 100 r (see Fig.16), and that the value of the momentum thickness is related to this ratio (see Appendix 2). It is not surprising, therefore, that conditions at the edge of the boundary layer, and the form of the boundary layer itself are different from those on a sharp cone in this region.

Static pressures on the surface were measured to see if these could have had a significant effect on the stability of the boundary layer (see Table 2 and Fig.9). It was found that all the measurements described were made in a region of essentially constant pressure. The only effect of the variation of static pressure which must occur nearer the blunt tip, is therefore on the structure of the boundary layer in that region.

2 APPARATUS

2.1 Tunnel facilities

The tests were carried out in a 5 in. x 5 in. supersonic tunnel at the R.A.E. Farnborough. Undisturbed free-stream Mach numbers of 3.12 and 3.81 were used in the tests, giving undisturbed free-stream Reynolds numbers per inch of 1.72×10^5 and 1.19×10^5 respectively per atmosphere of stagnation pressure. The stagnation pressure was varied between 1 and 5 atmospheres, and was held steady when necessary (as during a pitot traverse) to within ±0.1" Hg. The stagnation temperature, which was thermostatically controlled, was regulated in the early tests to be 41°C*; in later tests, it was found that the available supply of heat was insufficient to maintain this temperature, and in many tests the stagnation temperature was as low as 38°C.

2.2 Models

Five stainless steel models were prepared, each being a 15° included angle cone; the tips were ground to spherical radii up to half an inch. Some of the small-radius models were later blunted to intermediate radii, and altogether transition tests were carried out for cones with seven different nose radii. These are shown in Fig.3. Some of these cones were also used for pitot traverses of the boundary layer. Each cone had a single static pressure hole on the same generator used for the traverses.

Another cone was used to measure static pressures. This had a removable tip, and tips of five different radii could be fitted. Details, including the position of the pressure holes, are shown in Fig.4.

---

* This gives a recovery temperature approximately equal to room temperature.

2.3 Instrumentation

Most of the measurements of transition position were made from shadowgraph photographs of the flow. In some tests, schlieren photographs were also taken, and compared with the shadowgraphs; in all cases the two methods gave the same results. Transition position was measured to the nearest 0.1 inch. (The values of Reynolds number per inch are quoted in Table 1.)

The pressure in the settling chamber was measured with a Midwood capsule manometer, set to read pressures from 1 to 5 atmospheres. The manometer reading gave the absolute pressure in inches of mercury, and the instrument could be read to 0.01" Hg. In most cases, the stagnation pressure was maintained constant to the nearest 0.1" Hg.

The stagnation temperature was measured with a copper-constantan thermocouple in the settling chamber.

Static pressures were measured on a bank of manometers containing butyl phthalate; differences of pressure from a reference pressure were measured on this bank, and the reference pressure was measured on a mercury manometer balanced against atmosphere.

Traverses of the boundary layer were made with quartz pitot tubes of outside diameter about 0.007". This was found to be a suitable compromise between the small value needed because of the thinness of the boundary layer (in some cases 0.020" or even less) and the large internal diameter needed to enable the reading to become steady in a comparatively short time. The tubes used took between one and two minutes to attain a steady reading after being moved to a new station. The pitot pressure was measured to the nearest 0.01" Hg by means of a Midwood capsule manometer whose range was from 0 to 4 atmospheres.

3 TRANSITION RESULTS FROM SHADOWGRAPH

Shadowgraphs of the flow round each cone were taken at several stagnation pressures. The incidence of the cone was adjusted in each case so that transition positions on top and bottom generators were within 1 inch of each other; since some of the cones were tested on several separate occasions, greater accuracy of incidence setting would have been desirable but was found too time-consuming. In each case the mean of the two positions has been used in the analysis of results, and it is found that these are in agreement for the small variations of incidence involved.

At the higher Mach number, shocks from plugs in the upper liner struck the top surface of the cone and definitely promoted early transition in cases where the transition point was near the base of the cone. As a result, the experiments at a free-stream Mach number of 3.81 may be less reliable than those at a free-stream Mach number of 3.12.

The results of these tests are given in Table 1, and plotted in Figs.5 and 7. In Fig.5, the value of R_x at transition is shown as a function of u_∞/ν_∞, the Reynolds number per inch on the corresponding sharp cone under the same free stream conditions; the transition Reynolds number R_{x_t} is taken as $u_\infty x_t/\nu_\infty$ and is therefore the true Reynolds number only in the region where sharp cone conditions hold at the edge of the boundary layer (i.e. for $x > 100\ r$ as will be shown in section 4.3). In Fig.7, the position of transition, given by $x = x_t$, is shown as a function of u_∞/ν_∞. The actual distance s along the surface when $\alpha = 7\frac{1}{2}^\circ$ is given by

$$s = 1.0086\ x + 0.5629\ r$$

(see Fig.2 for notation), and this quantity varies from x by less than 5% for all the values of x and r used, and in most cases by less than 1%. The measured value of x_t is therefore supposed equal to the actual distance along the surface from tip to transition position.

Fig.5 shows that for most cones there is a tendency for the Reynolds number at transition to increase with Reynolds number per inch. The exceptions are the sharp cone when $M_o = 3.12$ (on which R_x is essentially independent of u_∞/ν_∞), and the two bluntest cones at the same value of M_o. From this figure it appears that for the smaller values of r, R_x increases with r for a given value of u_∞/ν_∞, but that the trend is reversed for r greater than about 0.062 in. when $M_o = 3.12$ or 0.048 in. when $M_o = 3.81$; the original trend appears again for even larger values of r, but there is little data in this region. This is illustrated more clearly in Fig.6 which is obtained by cross-plotting from Fig.5, and gives the variation of R_x with r at constant values of u_∞/ν_∞.

When this reversal in trend was discovered in the original analysis of tests at a limited number of values of u_∞/ν_∞, it was thought that experimental inaccuracies or disturbances in the tunnel might be contributory causes. Further tests, made over a wider range of values of u_∞/ν_∞ (as given in Fig.5), ruled out these causes and led to the investigation of the boundary layer development reported in section 4 below.

Meanwhile, the effects of disturbances at $M_o = 3.81$ may be largely eliminated by considering Fig.7, where the value of x_t is plotted against u_∞/ν_∞ on a logarithmic scale; it is found that this enables a straight line to be faired through the experimental points for $M_o = 3.12$. For $M_o = 3.81$, the value of x_t has a 'plateau' at about $6\frac{1}{2}$" for the sharper cones, and at a rather smaller value for the blunter cones. This corresponds exactly to the position on the cone where a shock wave from the upper liner hits the cone, and shows that transition is indeed promoted by this shock. A faired line has, however, been drawn through the points corresponding to transition positions upstream of this plateau, and it is not unreasonable to produce this line into the region downstream.

The faired lines (produced where necessary) are drawn on one graph (for each Mach number) in Fig.8. To avoid a confused diagram, the lines are given only for the region $x_t > 100$ r. (It should be noted that the only cones for which $x_t < 80$ r have tip radius 0.083" or 0.165" for $M_o = 3.12$ and 0.165" for $M_o = 3.81$).

Two conclusions can be drawn. The first is that for x_t greater than about 100 r, transition position moves downstream as the tip radius r increases as predicted by Moeckel's theory[1]. The second is that for x_t less than 100 r (and greater than about 80 r) there can be a reversal of this movement; this can be seen in Fig.9 by inspection of the lines for r = 0.062 in. and 0.083 in.

4 PRESSURE MEASUREMENTS

4.1 Static pressures

Table 2 gives the variation with x of static pressure, p_1, along the cone for five tip radii and for three free-stream stagnation pressures, and a typical curve is shown in Fig.9. Although this pressure does vary slightly with distance from the tip, the percentage change is very small. Transition always occurred in the region covered by these measurements, so that the assumption of constant pressure is justified. The effect of tip radius on transition position cannot therefore be explained by the induced static pressure distribution.

4.2 Pitot traversed techniques

For these tests, the stagnation pressure was chosen for each cone so that transition always occurred at roughly the same location relative to the tunnel (usually about 3 in. from the base on the cone): this eliminated effects due to irregularities in the flow. On most of the cones tested, 4 traverses were made - 2 in the laminar and 2 in the turbulent region of the boundary layer. For the blunter cones, several traverses were made at a lower stagnation pressure so that the boundary layers were entirely laminar. The static pressure for each traverse was taken to be the value measured at the single pressure hole in the cone, since all traverses were made in the region shown in section 4.1 to have uniform static pressure.

From the ratio of static to pitot pressure, the Mach number and velocity distributions through the boundary layer were found, and hence the displacement thickness δ_1 and the momentum thickness δ_2 were calculated. The local Reynolds number per inch at the edge of the boundary-layer was calculated from the values of static pressure, total temperature and measured Mach number at this point. Hence the Reynolds number R_{δ_2} based on momentum thickness was calculated.

The main uncertainty in this procedure arises in choosing the position of the "edge" of the boundary layer. In Fig.10 are sketches (not to the same scale) of the variations of pitot pressure across the boundary layer found for different values of x/r. Fig.10a shows the usual kind of profile in which p_o' increases rapidly with z at first, and then steadies to a constant value; this is the type of profile obtained for large values of x/r (x/r greater than about 100), and there is no difficulty in determining the edge of the boundary layer. Near to the tip (x/r of the order 10 or less) the profile is as shown in Fig.10c; here the value of p_o' steadies to a nearly constant value, and then starts increasing again as the probe traverses an external shear layer. Again there is no difficulty. For intermediate values of x/r, however, the profile is more like that in Fig.10b. In this profile, the value of p_o' begins to steady to a constant value, but before it reaches this value it begins to increase again because of the external shear layer; all that can be seen are the two points of inflection fairly close together, and the position of this region is difficult to determine exactly. In practice, the position was determined partly by a careful inspection of the graph, and partly by watching the dial of the pressure recorder while the measurements were being carried out: as the probe passed through these points of inflection, the needle of the recorder seemed to move more sluggishly than for smaller or larger values of z. Fairly good agreement was obtained between these two methods. Measured values of p_o' are shown in Fig.11 for typical traverses of the three types.

4.3 Conditions at edge of boundary layer

The value of M_1, the Mach number at the edge of the boundary layer, was calculated from the ratio of the pitot pressure there and the static pressure at the surface. These results are given in Table 3, and the values for laminar layers are plotted in Fig.12 (where x is less than 100 r) as a function of x/r. This correlates the results from the cones of different tip radii. It is clear that for small x/r, where the boundary layer is thin relative to the external shear layer, the value of M_1 approaches that given by Moeckel[1] for the surface of the cone. As x increases, M_1 increases to its sharp cone value which is in the region of x = 100 r. The corresponding values of $\rho_1 u_1/\mu_1 p_o$ are shown in Fig.13.

TABLE 2

Static pressures

(a) $M_o = 3.12$

	r ÷ 0			r ÷ 0.005"			r ÷ 0.05"			r ÷ 0.16"		
p_o ("Hg)	88.3	117.7	147.7	93.3	119.0	148.2	89.4	118.2	137.9	88.7	116.2	114.3
$\frac{p_1}{p_o}$ at A	0.0337	0.0309	0.0311	0.0305	0.0306	0.0313	0.0313	0.0307	0.0308	0.0300	0.0298	0.0295
B	0.0337	0.0310	0.0311	0.0318	0.0308	0.0316	0.0313	0.0309	0.0311	0.0302	0.0300	0.0300
C	0.0334	0.0307	0.0314	0.0300	0.0305	0.0316	0.0311	0.0308	0.0308	0.0302	0.0300	0.0299
D	B L O C K E D			B L O C K E D			B L O C K E D			B L O C K E D		
E	B R O K E N			B R O K E N			B R O K E N			B R O K E N		
F	0.0328	0.0306	0.0315	0.0293	0.0305	0.0311	0.0306	0.0302	0.0309	0.0299	0.0303	0.0296
G	0.0323	0.0300	0.0303	0.0287	0.0297	0.0303	0.0300	0.0298	0.0300	0.0296	0.0297	0.0297
H	0.0331	0.0305	0.0308	0.0297	0.0304	0.0309	0.0307	0.0306	0.0308	0.0302	0.0301	0.0300
I	0.0321	0.0295	0.0299	0.0293	0.0299	0.0303	0.0304	0.0300	0.0301	0.0305	0.0302	0.0300
J	0.0335	0.0311	0.0313	0.0295	0.0301	0.0304	0.0310	0.0307	0.0307	0.0309	0.0308	0.0304
K	0.0353	0.0327	0.0323	0.0303	0.0308	0.0308	0.0311	0.0308	0.0306	0.0310	0.0306	0.0305
L	0.0334	0.0307	0.0309	0.0304	0.0300	0.0306	0.0307	0.0302	0.0301	0.0306	0.0300	0.0299
M	0.0338	0.0310	0.0308	0.0301	0.0306	0.0308	0.0313	0.0306	0.0302	0.0311	0.0306	0.0299
N	0.0336	0.0308	0.0318	0.0296	0.0306	0.0313	0.0310	0.0306	0.0308	0.0311	0.0307	0.0306
O	0.0332	0.0311	0.0311	0.0306	0.0304	0.0306	0.0308	0.0301	0.0302	0.0311	0.0307	0.0303
P	0.0330	0.0304	0.0308	0.0295	0.0300	0.0307	0.0303	0.0303	0.0305	0.0305	0.0305	0.0309

For small changes of x/r, it is permissible to express any function of x/r in the form of a power law; hence,

$$\frac{u_1 \rho_1}{\mu_1 p_o} \propto \left(\frac{x}{r}\right)^m \quad \text{and} \quad \frac{p_o \delta_2^2}{r} \propto \left(\frac{x}{r}\right)^n$$

where m and n may vary slowly with x/r, but for small changes may be taken as constant. In this case,

$$R_{\delta_2} \propto \left(\frac{x}{r}\right)^{m+\frac{1}{2}n} r^{\frac{1}{2}} ;$$

and if transition occurs for a constant value of R_{δ_2}, then

$$\left(\frac{x_t}{r}\right)^{m+\frac{1}{2}n} \propto r^{-\frac{1}{2}}$$

i.e.
$$x_t \propto r^{1-\frac{\frac{1}{2}}{m+\frac{1}{2}n}} .$$

It follows that when $m+\frac{1}{2}n$ is greater than $\frac{1}{2}$, x_t increases with r; when $m+\frac{1}{2}n$ is less than $\frac{1}{2}$, however, x_t increases as r decreases. When $m+\frac{1}{2}n = \frac{1}{2}$, transition remains stationary as r varies. The theoretical curves (with measured Mach number distribution) show $m+\frac{1}{2}n$ greater than or equal to $\frac{1}{2}$, to that transition would be expected to move back always as r increases. The experimental curves, however, show the opposite tendency in one region. For x greater than about 100 r, $m+\frac{1}{2}n$ is greater than $\frac{1}{2}$ because $n = 1$ and m is positive; for x less than about 80 r (and greater than, say, 50 r) $m+\frac{1}{2}n$ is greater than $\frac{1}{2}$ because m is greater than $\frac{1}{2}$ and n is positive. But for the region where x is just under 100 r, both m and n are small, and $m+\frac{1}{2}n$ is less than $\frac{1}{2}$ (exact values are not quoted because of the insufficient information from Fig.13).

It seems, therefore, that the upstream movement of transition position as r increases in the region for x just less than 100 r is due to the large experimental values of δ_2 compared with theory in this region, and to the low experimental rate of change with x/r of $p_o \delta_2^2/r$.

It is shown in Appendix 2 that the ratio $\left(\int_0^x r_o^2\,dx \;\; r_o^2\, x\right)$ is related to the value of the momentum thickness on a blunt cone compared with that on the corresponding flat plate (given by the Mangler transformation). This quantity is shown in Fig.16 as a function of x/r for a 15^o blunt cone, and it can be seen that for x greater than 100 r, the ratio differs little from its sharp-cone value of $\frac{1}{3}$. It would appear, therefore, that the major difference in boundary layer properties on a blunt cone from those on a sharp cone would be expected to occur for x less than 100 r.

Finally it may be noted that conventional formulae for boundary layer growth assume that the streamwise velocity outside the boundary layer does not vary with distance from the surface, but only with distance along the surface. Figs.10 and 11 illustrate that this assumption is correct when x/r is large (considerably greater than 100) or small (around 10), but for intermediate values the assumption is not justified and we must consider the growth of a boundary layer under an external shear flow. An extension of the treatments of references 3 to 7 might be applicable to the present case, but this is beyond the scope of the present note.

5 CONCLUSIONS

(1) When x_t is greater than 100 r, x_t increases as r increases: i.e. the position of transition moves downstream as tip radius increases. When x_t is less than 100 r (and greater than about 80 r), this trend is reversed.

(2) When x is greater than 100 r, the conditions at the outer edge of the boundary layer are the same as those on a sharp cone, so that the downstream movement of transition is not associated with a reduced value of Reynolds number per inch. When x is less than 100 r the Reynolds number per inch at the outer edge of the boundary layer is less than on a sharp cone, but for 80 r < x < 100 r transition moves in the reverse direction (upstream) to that which might be expected.

(3) Transition occurs when $R_{\delta_2} \doteqdot 680$ when $M_o = 3.12$, and when $R_{\delta_2} \doteqdot 600$ when $M_o = 3.81$. This suggests that transition is caused by the usual kind of boundary-layer instability.

(4) Further experimental investigation of the conditions in the region near x = 100 r is necessary. Further theoretical work must include the consideration of boundary layer development in an external shear flow.

LIST OF SYMBOLS

a^*	sonic velocity
M_o	free stream Mach number (ahead of bow shock)
M_1	Mach number at edge of boundary layer
M_∞	value of M_1 on sharp cone
p_o	free stream stagnation pressure
p_1	static pressure on surface of cone
p_o'	pitot pressure
r	radius of tip of cone
r_o	distance of point on surface from axis of cone
$\bar{r}$	r_o/r
R_o	gas constant
R_{δ_2}	Reynolds number based on momentum thickness and true local conditions outside the boundary layer
$\left(R_{\delta_2}\right)_t$	value of R_{δ_2} at transition
R_x	Reynolds number based on x and conditions outside the boundary layer on a sharp cone
s	distance along surface of cone
T_o	stagnation temperature
T_1	temperature at edge of boundary layer
x	distance parallel to axis of point on surface from tip
X	x/r
x_t	value of x at transition
u_1	velocity at edge of boundary layer
u_∞	value of u_1 on sharp cone
α	semi-vertex angle of cone
γ	ratio of specific heats
δ_1	displacement thickness of boundary layer
δ_2	momentum thickness of boundary layer
μ_o	viscosity under stagnation conditions
μ_1	viscosity at edge of boundary layer
ν_o	kinematic viscosity under stagnation conditions
ν_1	kinematic viscosity at edge of boundary layer
ν_∞	value of ν_1 on sharp cone
ρ_o	free stream stagnation density
ρ_1	density at edge of boundary layer
ρ_∞	value of ν_1 on sharp cone

LIST OF REFERENCES

No.	Author	Title, etc.
1	Moeckel, W.E.	Some effects of bluntness on boundary-layer transition and heat transfer at supersonic speeds. NACA Rept.1312 (Supersedes NACA TN 3653), 1957.
2	Rott, N. Crabtree, L.F.	Simplified laminar boundary-layer calculations for bodies of revolution and for yawed wings. J. Aero. Sci. 19(8) pp.553-565, August 1952.
3	Li, T.Y.	Simple shear flow past a flat plate in an incompressible fluid of small viscosity. J. Aero. Sci. 22(9) pp.651-652, September 1955.
4	Li, T.Y.	Simple shear flow past a flat plate in a compressible viscous fluid. J. Aero. Sci. 22(10) pp.724-725, October 1955.
5	Yen, K.T.	Approximate solutions of the incompressible laminar boundary layer equations for a flat plate in a shear flow. J. Aero. Sci. 22(10) pp.728-730, October 1955.
6	Glauert, M.B.	The boundary layer in simple shear flow past a flat plate. J. Aero. Sci. 24(11) pp.848-849, November 1957.
7	Murray, J.D.	The boundary layer on a flat plate when the main stream has uniform shear. TIL No. P75170. Division of Engineering and Applied Physics, Harvard University, June 1958.

APPENDIX 1

VARIATION WITH $\frac{x}{r}$ OF $\frac{\rho_1 u_1}{p_o \mu_1}$ AND $\frac{p_o \delta_2^2}{r}$

If the variation of M_1 with x at the edge of the boundary layer is due primarily to the convergence of the streamlines towards the conical surface (rather than to the increase in thickness of the boundary layer), then M_1 must be a function of x/r. That this is so is borne out by Fig.12.

It follows immediately that $\rho_1 u_1/p_o \mu_1$ is a function of x/r only for given free-stream Mach number and stagnation temperature, since

$$\frac{\rho_1 u_1}{p_o \mu_1} = \left(\frac{\gamma}{RT_o}\right) \frac{p}{p_o} \left(\frac{T_1}{T_o}\right)^{-\frac{1}{2}} \frac{M_1}{\mu_1(T_1)} \qquad (1)$$

where p is the static pressure on the surface of the corresponding sharp cone. All the quantities on the right hand side of (1) are functions of M_1 and M_o and T_o only.

With the same assumptions, it can be shown that $p_o \delta_2^2/r$ is a function of x/r only for given M_o and T_o. For, using the formula given by Rott and Crabtree[2]

$$\delta_2^2 = 0.45 \nu_o \left(\frac{T_1}{T_o}\right)^{-3} u_1^{-6} r_o^{-2} \int_o^s \left(\frac{T_1}{T_o}\right)^{1.5} u_1^5 r_o^2 \, ds , \qquad (2)$$

and introducing the non-dimensional variables

$$\bar{r}_o = \frac{r_o}{r} , \qquad \bar{s} = \frac{s}{r} , \qquad M_1^* = \frac{u_1}{a^*} \qquad (3)$$

where a* is the sonic velocity of the free stream,

$$\frac{p_o \delta_2^2}{r} = 0.45 RT_o \mu_o(T_o) a^{*-1} (T_o) \left(\frac{T_1}{T_o}\right)^{-3} M_1^{*-6} \bar{r}_o^{-2} \int_o^{\bar{s}} \left(\frac{T_1}{T_o}\right)^{1.5} M_1^{*5} \bar{r}_o^2 \, d\bar{s} .$$

Since all the quantities in (3) are functions of x/r only, and so is M_1, it follows that $p_o \delta_2^2/r$ is a function of x/r, M_o and T_o only.

APPENDIX 2

THE MANGLER TRANSFORMATION

This is given for a general body of revolution by the by the relations

$$\bar{s} = \frac{1}{A^2}\int_0^s r_o^2\, ds\,, \qquad \bar{z} = \frac{r_o}{A}\, z$$

where A is an arbitrary reference length, and the barred quantities indicate values on the corresponding flat plate (with pressure gradient). At corresponding points on the body of revolution and the flat plate, the momentum thicknesses are given by

$$\bar{\delta}_2 = \int_0^\infty \frac{\bar{\rho}\,\bar{u}}{\bar{\rho}_1\,\bar{u}_1}\left(1 - \frac{\bar{u}}{\bar{u}_1}\right) d\bar{z} = \int_0^\infty \frac{\rho u}{\rho_1 u_1}\left(1 - \frac{u}{u_1}\right)\frac{r_o}{A}\, dz = \frac{r_o}{A}\,\delta_2 .$$

It follows that

$$\frac{\delta_2^2}{s} = \left(\frac{\delta_2}{\bar{\delta}_2}\right)^2 \left(\frac{\bar{s}}{s}\right)\frac{\bar{\delta}_2^2}{\bar{s}} = \left(\frac{1}{s r_o^2}\int_0^s r_o^2\, ds\right)\frac{\bar{\delta}_2^2}{\bar{s}} .$$

The factor $\left(\int_0^s r_o^2\, ds\right) \Big/ s r_o^2$ is plotted in Fig.16 as a function of s/r for a blunt 15° cone. It is seen that for x greater than about 100 r, the factor is very little different from its value for a sharp cone; for x less than 100 r, there is a considerable variation from the sharp cone value.

Alternatively, manipulation of the Rott and Crabtree formula quoted in Appendix 1 gives

$$\frac{R_{\delta_2}^2}{R_{1x}} = 0.45\left[\frac{\int_0^s M_1^5\left(\frac{T_1}{T_o}\right)^4 r_o^2\, ds}{M_1^5\left(\frac{T_1}{T_o}\right)^4 r_o^2\, s}\right],$$

where R_{1x} is the Reynolds number based on local conditions and x. The quantity in square brackets has been calculated using the measured values of M_1, and is shown in the table below: it is clear that for x/r greater than 10, it is negligibly different from the simpler ratio $\int_0^s r_o^2\,ds \Big/ r_o^2\,s$.

$\frac{x}{r}$	$\left[\int_0^s M_1^5 \left(\frac{T_1}{T_o}\right)^4 r_o^2\,ds \Big/ M_1^5 \left(\frac{T_1}{T_o}\right)^4 r_o^2\,s\right]$		$\int_0^s r_o^2\,ds \Big/ r_o^2\,s$
	$M_o = 3.12$	$M_o = 3.81$	
2	0.67	0.78	0.55
5	0.57	0.56	0.57
10	0.50	0.51	0.50
20	0.42	0.43	0.43
50	0.37	0.38	0.38
100	0.35	0.37	0.36
200	0.35	0.35	0.34
500	0.34	0.35	0.34
1000	0.34		0.33

TABLE 1

Transition position

(a) $M_o = 3.12$

x_t = distance in inches of transition position from tip

u_∞/ν_∞ = theoretical Reynolds number per inch at edge of boundary layer on sharp cone

Cone 0A r = 0.0003"		Cone 1 r = 0.0053"		Cone 3 r = 0.048"		Cone 1B r = 0.062"		Cone 2A r = 0.083"		Cone 0B r = 0.165"		Cone 7 r = 0.49"	
x_t	u_∞/ν_∞	x_t	u_∞/ν_∞	x_t	u_∞/ν_∞	x_t	u_∞/ν_∞	x_t	u_∞/ν_∞	x_t	u_∞/ν_∞	x_t	u_∞/ν_∞
7.1	3.81×10^5	7.6	3.21×10^5	> 7.6	3.88×10^5	> 7.7	4.79×10^5	> 7.5	5.04×10^5	> 6.8	5.16×10^5	> 5.4	8.40×10^5
6.1	4.44	6.3	4.39	6.6	4.88	6.5	5.75	7.1	5.59	6.6	5.68	5.4	8.70
5.7	4.90	6.6	4.40	6.6	5.06	6.0	6.32	6.1	6.11	6.6	6.29		
5.3	5.07	5.8	4.88	5.7	5.64	5.5	6.88	5.6	6.21	6.1	6.79		
5.7	5.07	5.5	5.15	6.0	5.80	5.4	7.10	5.6	6.22	5.4	7.37		
5.2	5.40	5.3	5.17	5.6	5.94	4.9	7.81	5.4	6.29	4.7	8.05		
4.4	6.23	5.7	5.18	5.8	6.18	4.7	8.38	5.5	6.66	4.5	8.40		
4.4	6.33	5.3	5.20	5.2	6.34			4.8	7.28				
3.6	7.26	5.3	5.29	5.3	6.73			4.5	7.48				
3.6	7.32	5.4	5.58	5.2	7.21			4.5	7.76				
3.1	8.47	4.6	6.24	4.7	7.51			4.0	8.24				
3.1	8.59	4.6	6.75	4.4	8.21			3.7	8.86				
		4.5	6.87	4.4	8.47								
		4.2	7.35										
		3.9	8.46										
		4.0	8.49										
		3.6	8.64										

TABLE 1 (Contd)

(b) $M_o = 3.81$

x_t = distance in inches of transition position from tip

u_∞/ν_∞ = theoretical Reynolds number per inch at edge of boundary layer on sharp cone

Cone 0A r = 0.0003"		Cone 1 r = 0.0053"		Cone 3 r = 0.048"		Cone 1B r = 0.062"		Cone 2A r = 0.083"		Cone 0B r = 0.165"		Cone 7 r = 0.49"	
x_t	u_∞/ν_∞	x_t	u_∞/ν_∞	x_t	u_∞/ν_∞	x_t	u_∞/ν_∞	x_t	u_∞/ν_∞	x_t	u_∞/ν_∞	x_t	u_∞/ν_∞
6.9	2.94×10^5	7.5	2.85×10^5	> 7.2	4.29×10^5	> 7.4	3.86×10^5	7.1	3.27×10^5	> 6.6	3.98×10^5	> 5.4	6.33×10^5
6.7	3.44	7.0	3.27	6.8	4.49	6.6	4.16	6.5	3.54	6.2	4.11		
6.6	3.51	6.5	3.88	6.8	4.53	6.4	4.65	6.5	4.17	6.2	4.43		
6.0	3.87	6.2	4.08	6.7	4.86	6.3	5.03	6.6	4.21	6.3	4.48		
5.7	4.49	5.7	4.45	6.4	5.44	6.0	5.54	6.1	4.35	5.9	4.85		
5.2	4.70	5.7	4.64	6.1	5.93	5.5	5.83	6.2	4.72	6.0	4.93		
4.4	5.72	5.3	5.09	5.8	6.00	5.2	6.25	6.1	5.17	5.8	5.31		
4.0	6.39	4.7	5.75	6.0	6.24			5.7	5.43	5.9	5.39		
		4.5	6.06	5.7	6.33			5.5	5.68	5.7	5.69		
								5.3	5.85	5.2	5.79		
								4.9	5.85	5.2	6.24		
								5.6	5.87	5.1	6.29		
								4.8	6.09				

TABLE 2

Static pressures

(a) $M_o = 3.12$

	r ÷ 0			r ÷ 0.005"			r ÷ 0.05"			r ÷ 0.16"		
p_o ("Hg)	88.3	117.7	147.7	93.3	119.0	148.2	89.4	118.2	137.9	88.7	116.2	114.3
$\frac{p_1}{p_o}$ at A	0.0337	0.0309	0.0311	0.0305	0.0306	0.0313	0.0313	0.0307	0.0308	0.0300	0.0298	0.0295
B	0.0337	0.0310	0.0311	0.0318	0.0308	0.0316	0.0313	0.0309	0.0311	0.0302	0.0300	0.0300
C	0.0334	0.0307	0.0314	0.0300	0.0305	0.0316	0.0311	0.0308	0.0308	0.0302	0.0300	0.0299
D	B L O C K E D			B L O C K E D			B L O C K E D			B L O C K E D		
E	B R O K E N			B R O K E N			B R O K E N			B R O K E N		
F	0.0328	0.0306	0.0315	0.0293	0.0305	0.0311	0.0306	0.0302	0.0309	0.0299	0.0303	0.0296
G	0.0323	0.0300	0.0303	0.0287	0.0297	0.0303	0.0300	0.0298	0.0300	0.0296	0.0297	0.0297
H	0.0331	0.0305	0.0308	0.0297	0.0304	0.0309	0.0307	0.0306	0.0308	0.0302	0.0301	0.0300
I	0.0321	0.0295	0.0299	0.0293	0.0299	0.0303	0.0304	0.0300	0.0301	0.0305	0.0302	0.0300
J	0.0335	0.0311	0.0313	0.0295	0.0301	0.0304	0.0310	0.0307	0.0307	0.0309	0.0308	0.0304
K	0.0353	0.0327	0.0323	0.0303	0.0308	0.0308	0.0311	0.0308	0.0306	0.0310	0.0306	0.0305
L	0.0334	0.0307	0.0309	0.0304	0.0300	0.0306	0.0307	0.0302	0.0301	0.0306	0.0300	0.0299
M	0.0338	0.0310	0.0308	0.0301	0.0306	0.0308	0.0313	0.0306	0.0302	0.0311	0.0306	0.0299
N	0.0336	0.0308	0.0318	0.0296	0.0306	0.0313	0.0310	0.0306	0.0308	0.0311	0.0307	0.0306
O	0.0332	0.0311	0.0311	0.0306	0.0304	0.0306	0.0308	0.0301	0.0302	0.0311	0.0307	0.0303
P	0.0330	0.0304	0.0308	0.0295	0.0300	0.0307	0.0303	0.0303	0.0305	0.0305	0.0305	0.0309

TABLE 2 (Contd)

(b) $M_o = 3.81$

	r ≑ 0			r ≑ 0.005"			r ≑ 0.05"			r ≑ 0.08"			r ≑ 0.16"		
p_o ("Hg)	95.1	131.6	157.2	90.5	121.8	152.8	94.1	118.7	151.9	92.6	124.5	156.2	91.7	129.3	155.2
$\frac{p_1}{p_o}$ at A	0.0144	0.0142	0.0142	0.0144	0.0142	0.0141	0.0138	0.0141	0.0140	0.0143	0.0140	0.0138	0.0133	0.0135	0.0132
B	0.0144	0.0142	0.0141	0.0144	0.0142	0.0140	0.0138	0.0140	0.0140	0.0143	0.0140	0.0138	0.0135	0.0136	0.0133
C	0.0139	0.0137	0.0137	0.0140	0.0138	0.0139	0.0135	0.0138	0.0137	0.0140	0.0138	0.0136	0.0134	0.0135	0.0133
D	0.0140	0.0138	0.0139	0.0141	0.0138	0.0140	0.0136	0.0139	0.0140	0.0140	0.0139	0.0139	0.0136	0.0137	0.0137
E	BROKEN			BROKEN			BROKEN			BROKEN			BROKEN		
F	0.0139	0.0136	0.0137	0.0140	0.0136	0.0137	0.0135	0.0137	0.0137	0.0140	0.0138	0.0137	0.0137	0.0138	0.0135
G	0.0143	0.0142	0.0141	0.0143	0.0141	0.0141	0.0138	0.0140	0.0140	0.0144	0.0141	0.0140	0.0140	0.0141	0.0139
H	BLOCKED			BLOCKED			BLOCKED			BLOCKED			BLOCKED		
I															
J	0.0146	0.0141	0.0143	0.0145	0.0141	0.0142	0.0140	0.0142	0.0143	0.0145	0.0142	0.0143	0.0142	0.0142	0.0143
K	0.0135	0.0133	0.0135	0.0132	0.0131	0.0133	0.0128	0.0131	0.0133	0.0135	0.0132	0.0133	0.0134	0.0133	0.0133
L	0.0139	0.0134	0.0135	0.0139	0.0138	0.0134	0.0135	0.0135	0.0134	0.0140	0.0134	0.0133	0.0133	0.0132	0.0130
M	0.0137	0.0132	0.0133	0.0137	0.0133	0.0134	0.0133	0.0134	0.0134	0.0138	0.0133	0.0134	0.0133	0.0133	0.0133
N	0.0137	0.0137	0.0143	0.0137	0.0135	0.0140	0.0133	0.0136	0.0138	0.0139	0.0136	0.0138	0.0137	0.0138	0.0138
O	0.0137	0.0139	0.0143	0.0137	0.0137	0.0141	0.0135	0.0137	0.0141	0.0140	0.0137	0.0141	0.0137	0.0139	0.0141
P	0.0141	0.0140	0.0143	0.0140	0.0139	0.0141	0.0135	0.0140	0.0142	0.0140	0.0139	0.0142	0.0138	0.0141	0.0142

TABLE 3

Boundary layer traverses

(a) $M_o = 3.12$

r(in.)	x_t(in.)	p_o("Hg)	x(in.)	M_1	δ_1(in.)	δ_2(in.)	$\frac{\rho_1 m_1}{\mu_1}$(in.$^{-1}$)	R_{δ_2}	approx. $(R_{\delta_2})_t$
0.0003	5.8	85	3.8	2.94	7.61×10^{-3}	0.86×10^{-3}	5.25×10^{5}	451	650
			4.7	2.92	9.36	1.04	5.13	534	
			5.8	2.88	7.47	1.35	4.92	665	
			6.7	2.91	12.64	2.33	5.10	1090	
0.0053	5.3	92	3.9	2.93	7.80	0.93	5.55	516	680
			4.75	2.94	8.30	1.13	5.53	626	
			5.8	2.83	9.25	1.59	5.00	795	
			6.75	2.96	13.61	2.49	5.66	1410	
0.048	5.5	104	3.6	2.79	5.86	0.94	5.71	537	700
			4.4	2.92	8.02	1.00	6.43	643	
			5.6	2.95	8.48	1.24	6.62	821	
			6.4	2.99	10.42	1.94	7.00	1360	
0.083	5.3	108	3.5	2.43	5.24	0.93	4.02	374	680
			4.2	2.50	6.73	1.16	4.28	4497	
			5.4	2.74	9.36	1.85	5.45	1010	
			6.2	2.92	15.55	2.81	6.49	1820	
0.165	6.5	105.5	3.7	2.30	11.0	1.70	3.36	571	?
			5.5	2.36	13.3	2.00	3.55	710	
0.49	> 5.4	105.5	3.4	2.21	11.4	1.86	3.04	565	?
			5.4	2.23	13.9	2.24	3.07	688	

TABLE 3 (Contd)

(b) $M_o = 3.81$

r(in.)	x_t(in.)	p_o("Hg)	x(in.)	M_1	δ_1(in.)	δ_2(in.)	$\frac{\rho_1 u_1}{\mu_1}$(in.$^{-1}$)	R_{δ_2}	approx. $(R_{\delta_2})_t$
0.0003	5.8	111	3.9	3.31	0.76×10^{-2}	0.86×10^{-3}	4.50×10^{5}	387	550
			4.8	3.36	0.86	0.98	4.65	420	
			5.9	3.30	1.02	1.37	4.43	608	
			6.8	3.37	1.51	2.21	4.70	1040	
0.048	5.5	145	3.6	2.95	0.97	1.08	4.16	450	620
			4.4	3.13	0.81	1.09	5.04	550	
			5.5	3.22	0.85	1.19	5.58	664	
			6.3	3.21	1.26	1.86	5.58	1040	
0.083	4.6	143	3.2	2.64	0.77	1.29	3.03	391	550
			4.2	2.78	1.08	1.45	3.51	509	
			5.2	3.25	1.30	1.86	5.56	1070	
			6.2	3.33	1.66	2.54	5.97	1520	
0.165	> 6.5	100	5.5	2.61	0.92	1.63	2.02	330	?
0.49	> 5.4	91.5	3.4	2.32	1.68	2.38	1.36	324	?
			5.4	2.34	1.74	2.73	1.39	380	

WT.2078.C.P.598.K3 - Printed in England

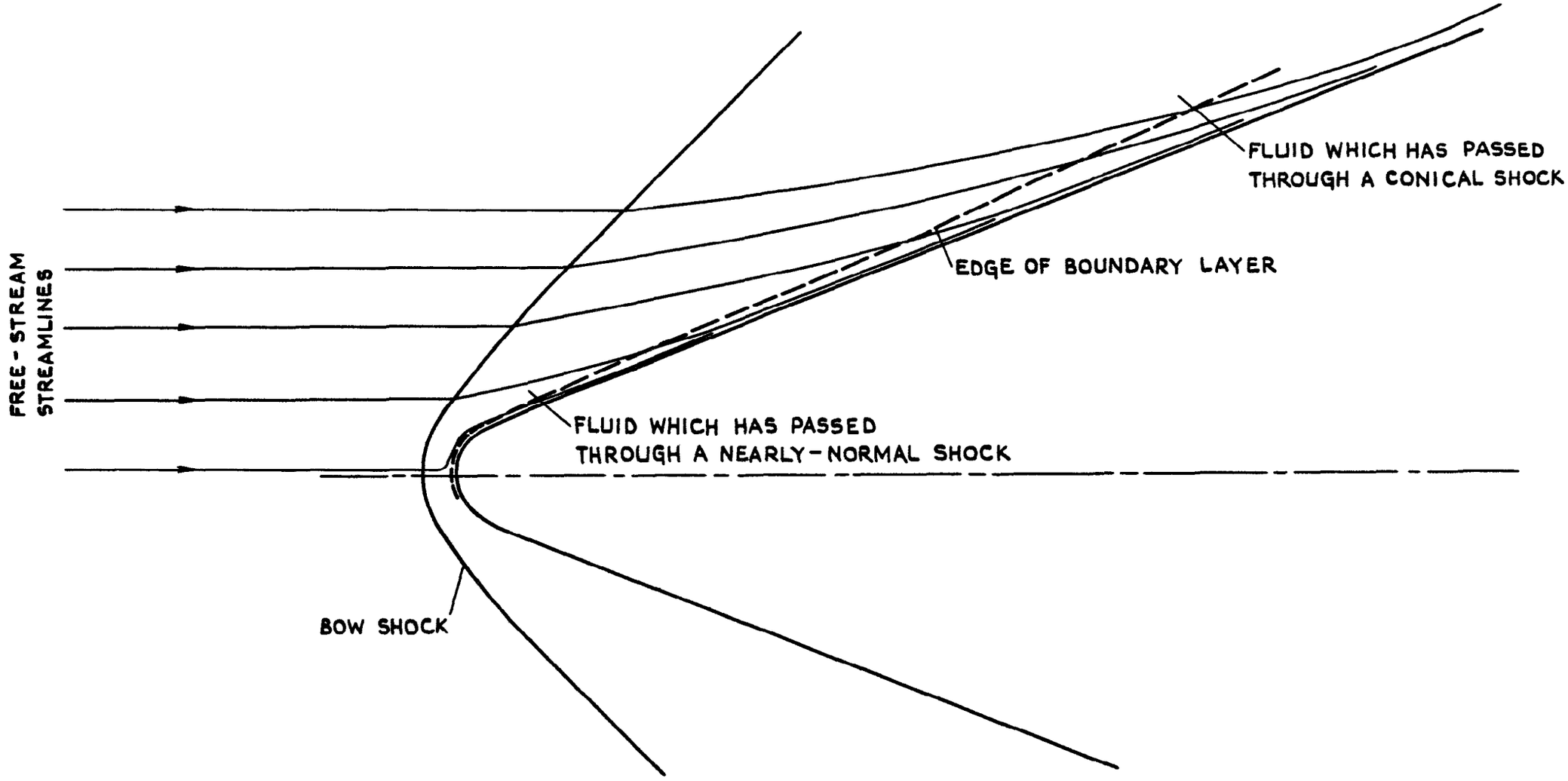

FIG.1. VARIATION IN CONDITIONS AT THE EDGE OF THE BOUNDARY LAYER ON A BLUNT CONE.

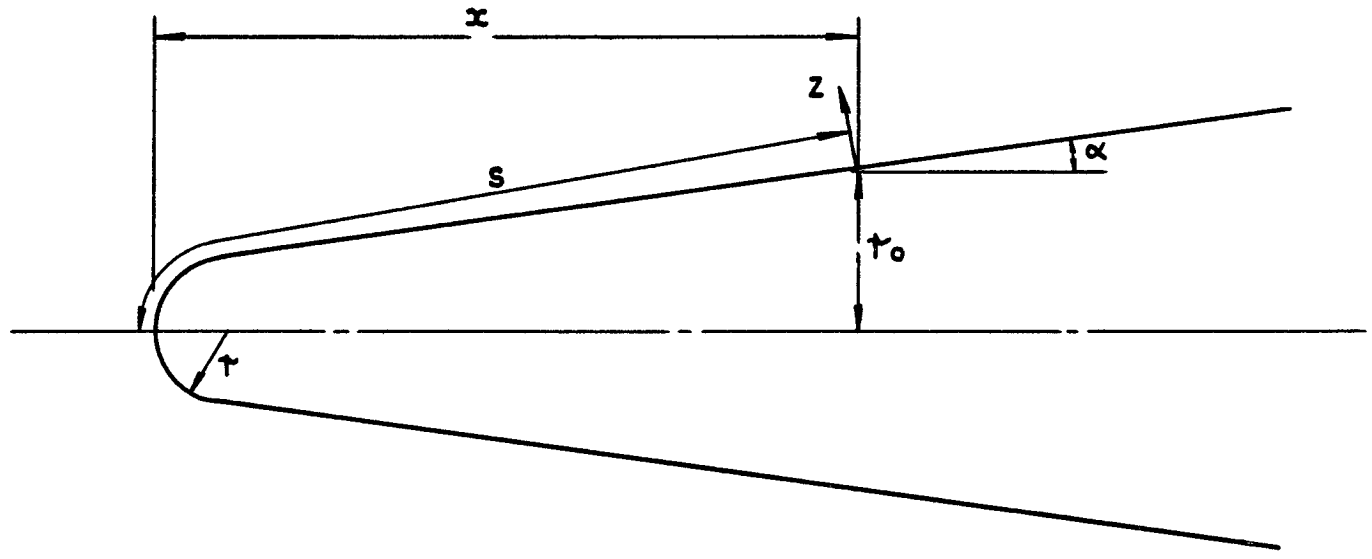

FIG.2. NOMENCLATURE FOR A BLUNT CONE.

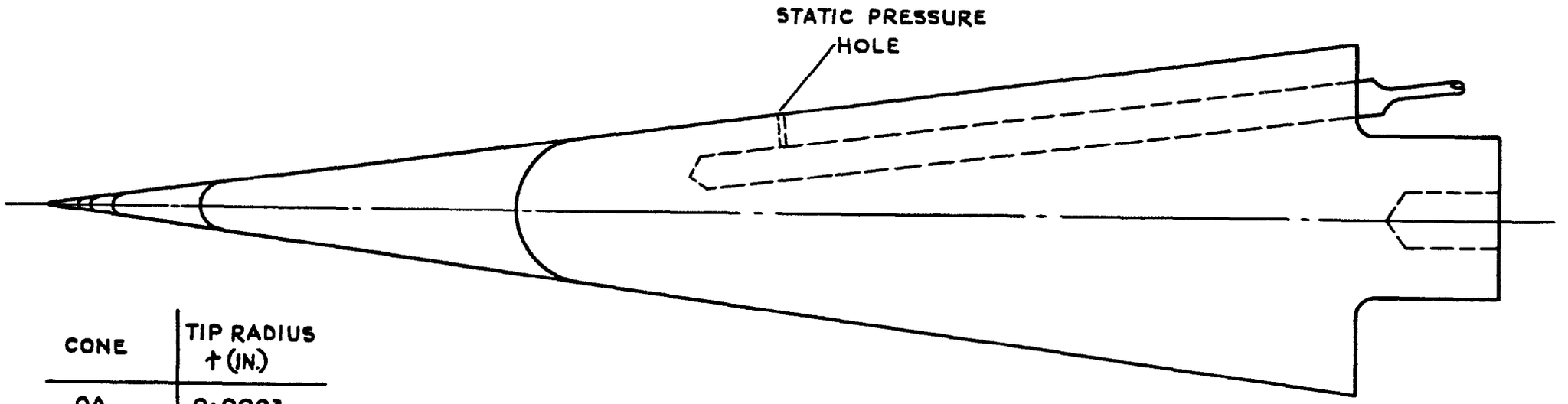

CONE	TIP RADIUS † (IN.)
0A	0·0003
1	0·0053
3	0·048
1B	0·062
2A	0·083
0B	0·165
7	0·49

FIG. 3. CONES USED FOR MEASUREMENT OF TRANSITION POSITION AND FOR PITOT TRAVERSES.

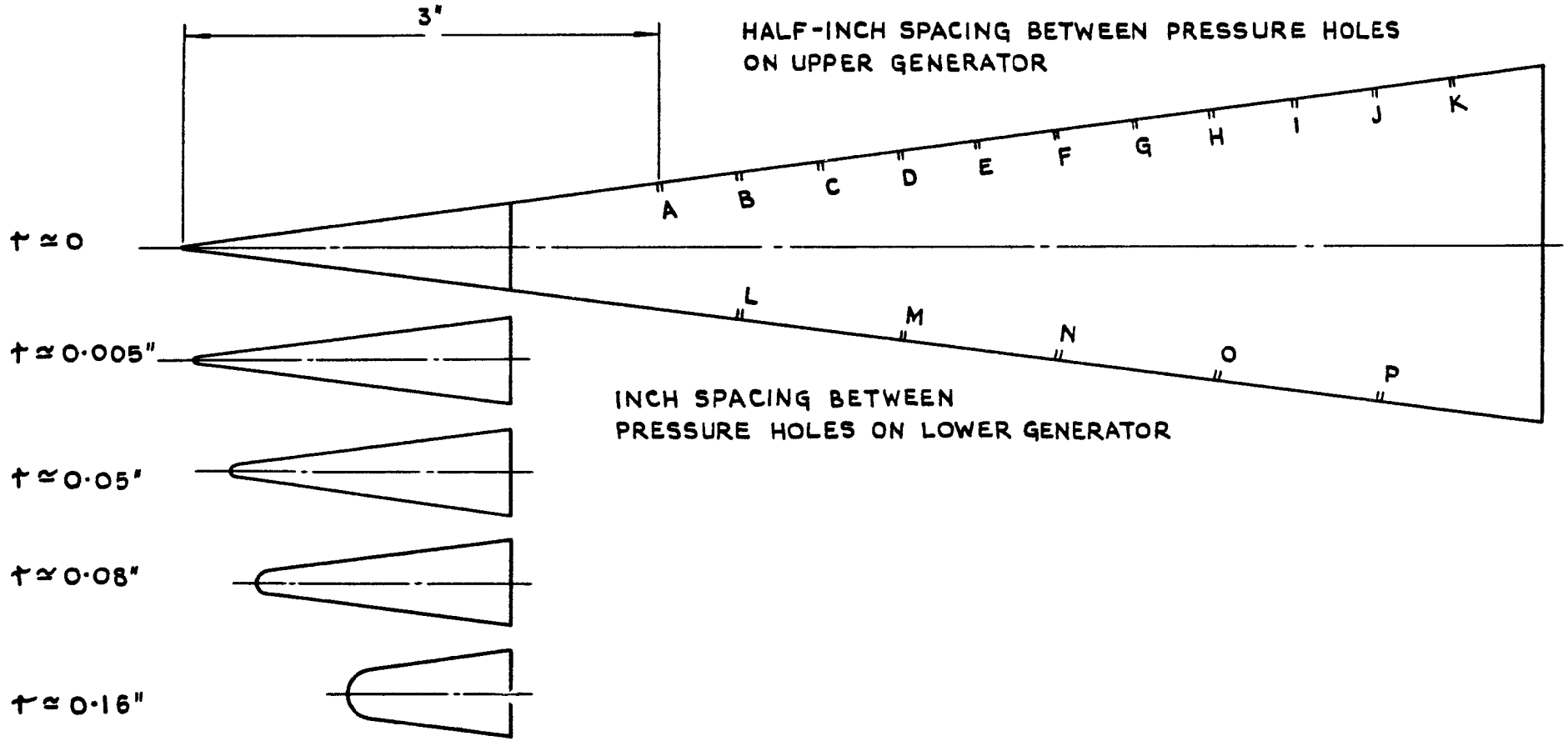

FIG.4. CONE WITH FIVE REMOVABLE TIPS USED FOR MEASURING STATIC PRESSURES.

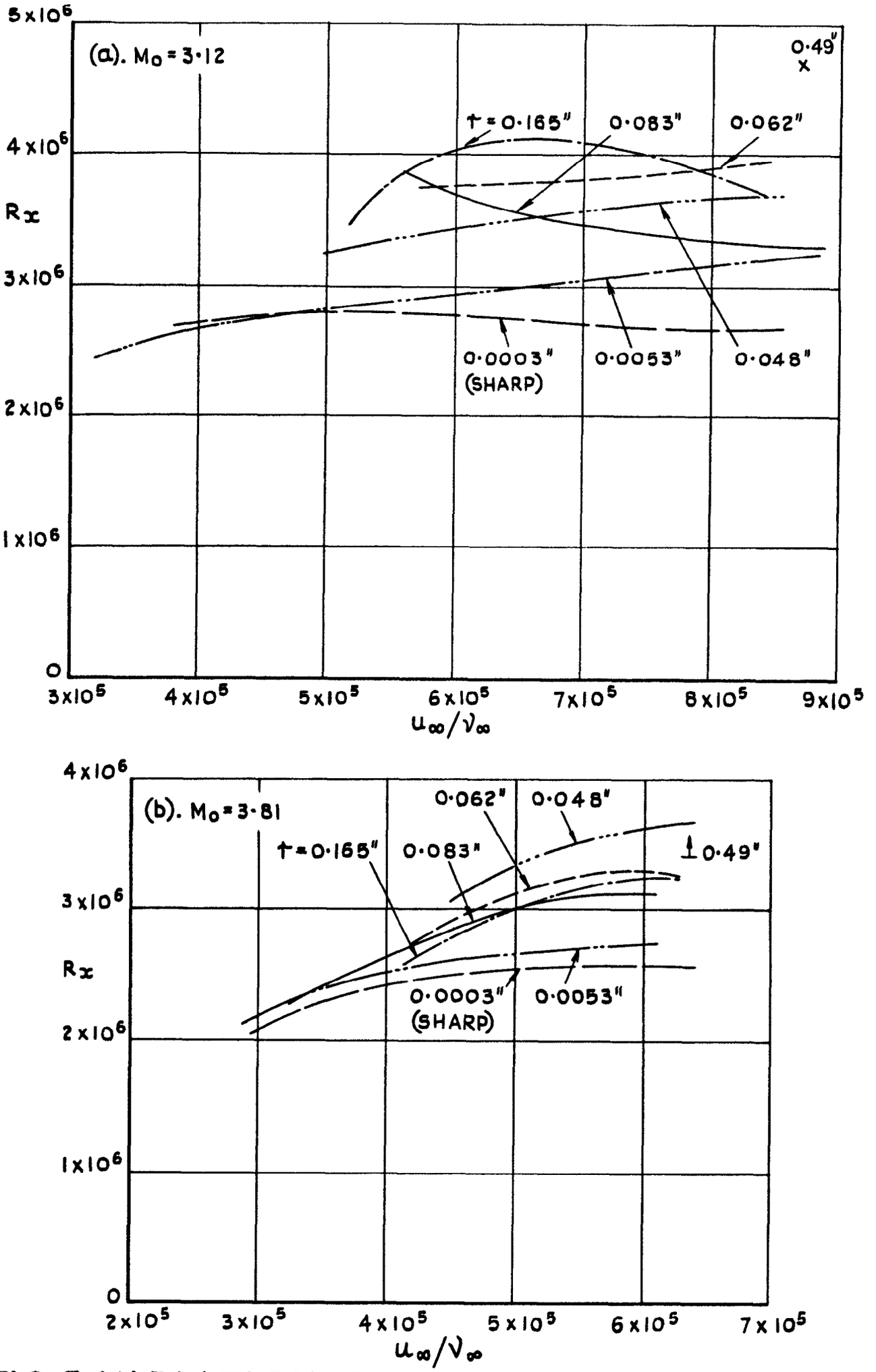

FIG.5. VARIATION OF REYNOLDS NUMBER, R_x, AT TRANSITION WITH REYNOLDS NUMBER PER INCH u_∞/ν_∞. (a). $M_0 = 3{\cdot}12$, (b). $M_0 = 3{\cdot}81$.

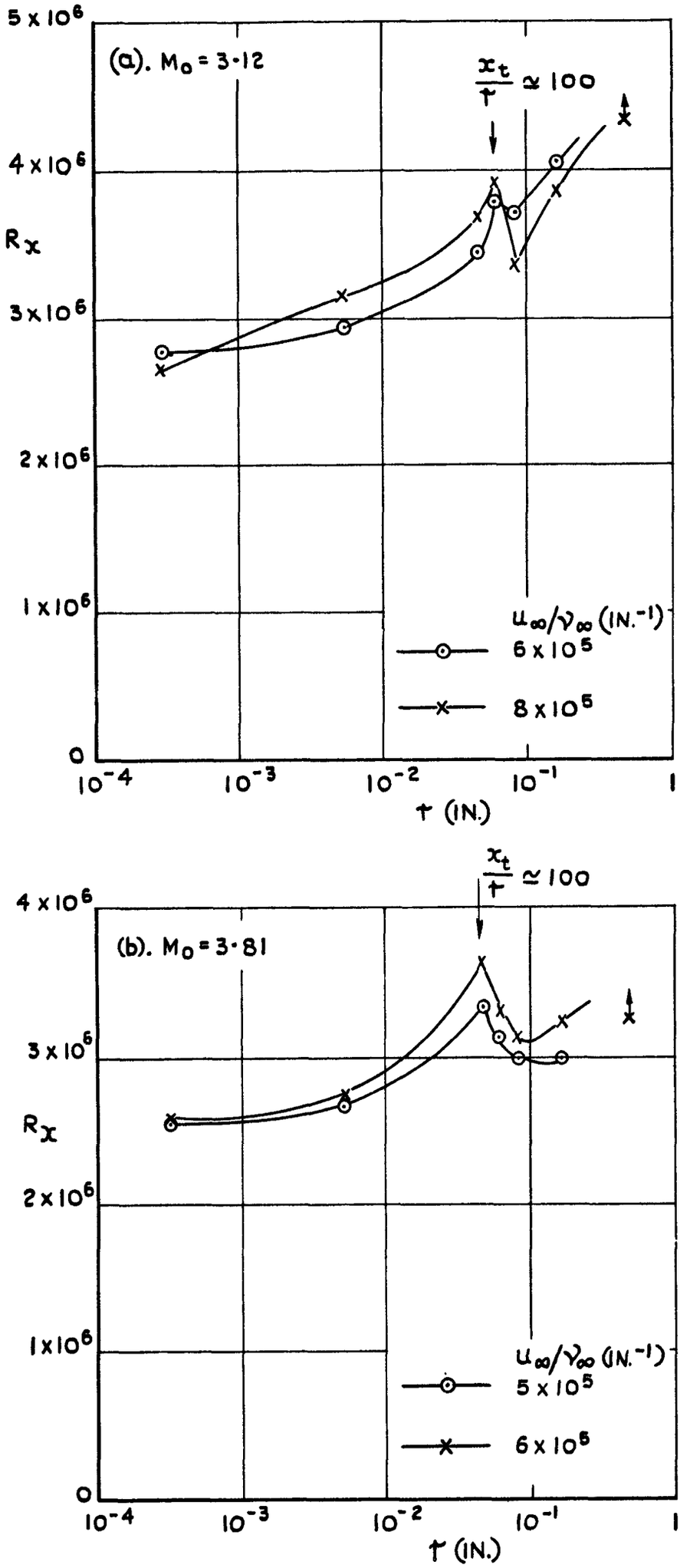

FIG.6. VARIATION OF REYNOLDS NUMBER, R_x, AT TRANSITION WITH TIP RADIUS, r.
(a). $M_0 = 3{\cdot}12$, (b). $M_0 = 3{\cdot}81$.

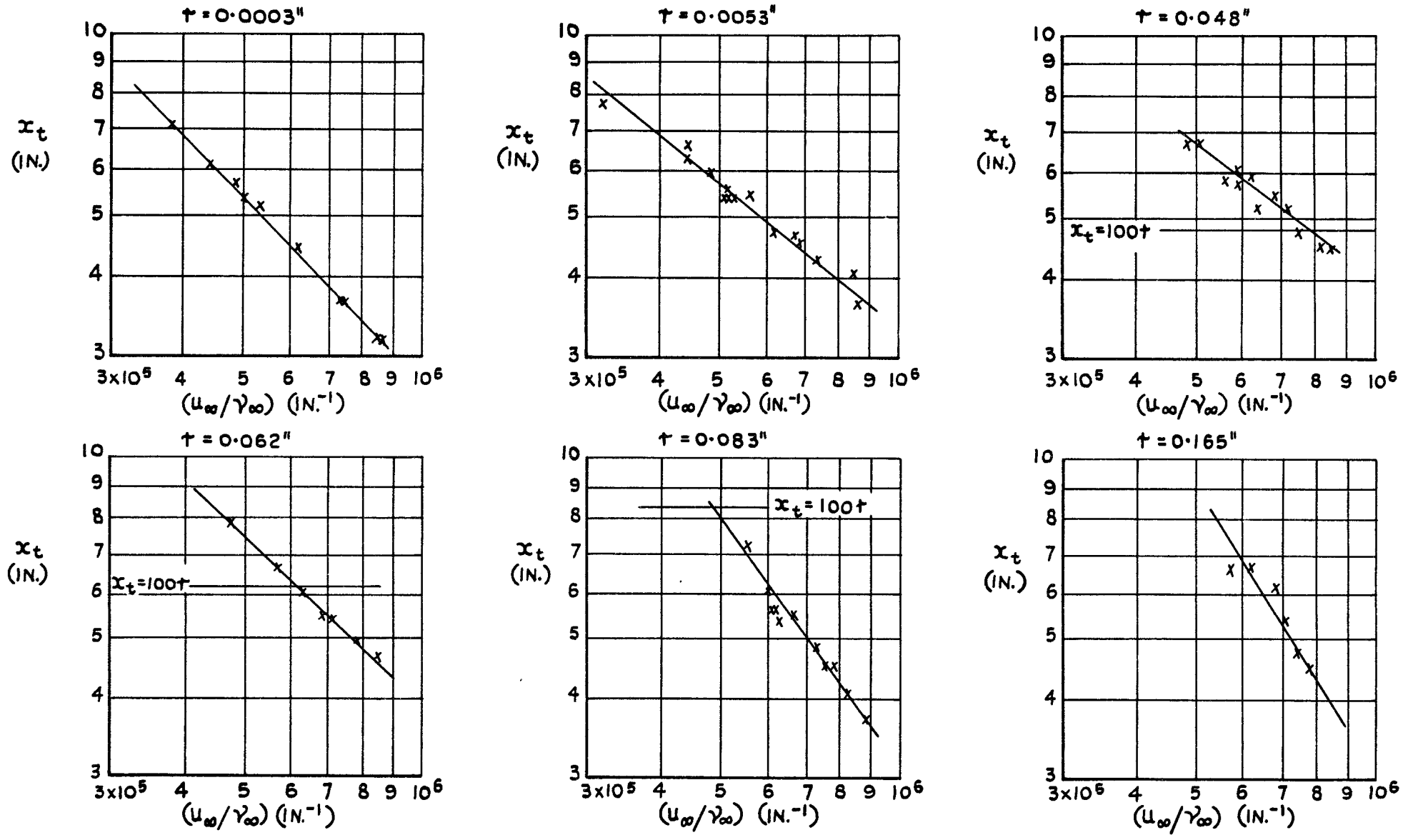

FIG.7. VARIATION OF MEASURED TRANSITION POSITION, x_t, WITH REYNOLDS NUMBER PER INCH, (u_∞/ν_∞), CALCULATED FOR A SHARP CONE.
(a). $M_o = 3{\cdot}12$.

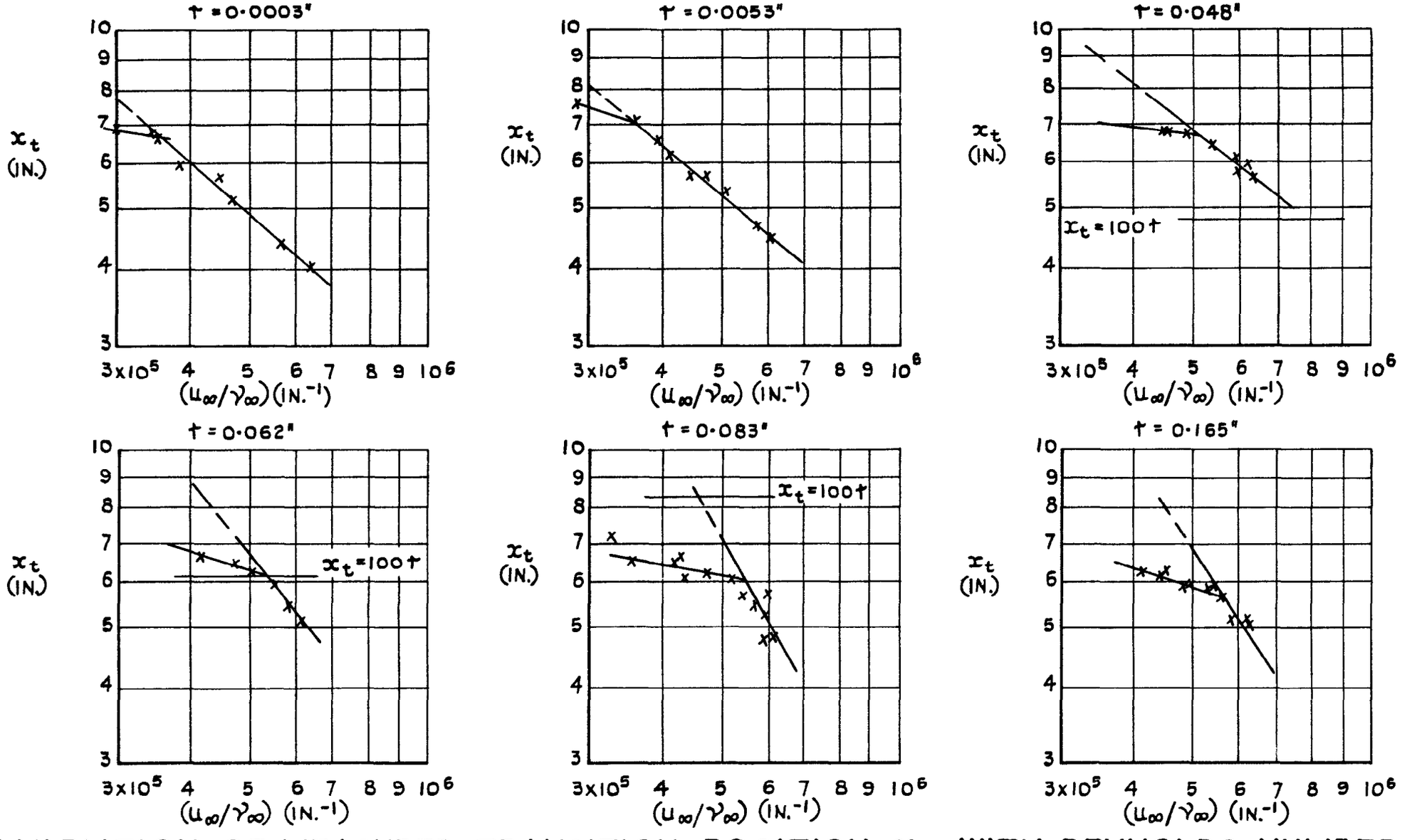

FIG.7. VARIATION OF MEASURED TRANSITION POSITION, x_t, WITH REYNOLDS NUMBER PER INCH, (u_∞/ν_∞), CALCULATED FOR A SHARP CONE.

(b). $M_o = 3 \cdot 81$.

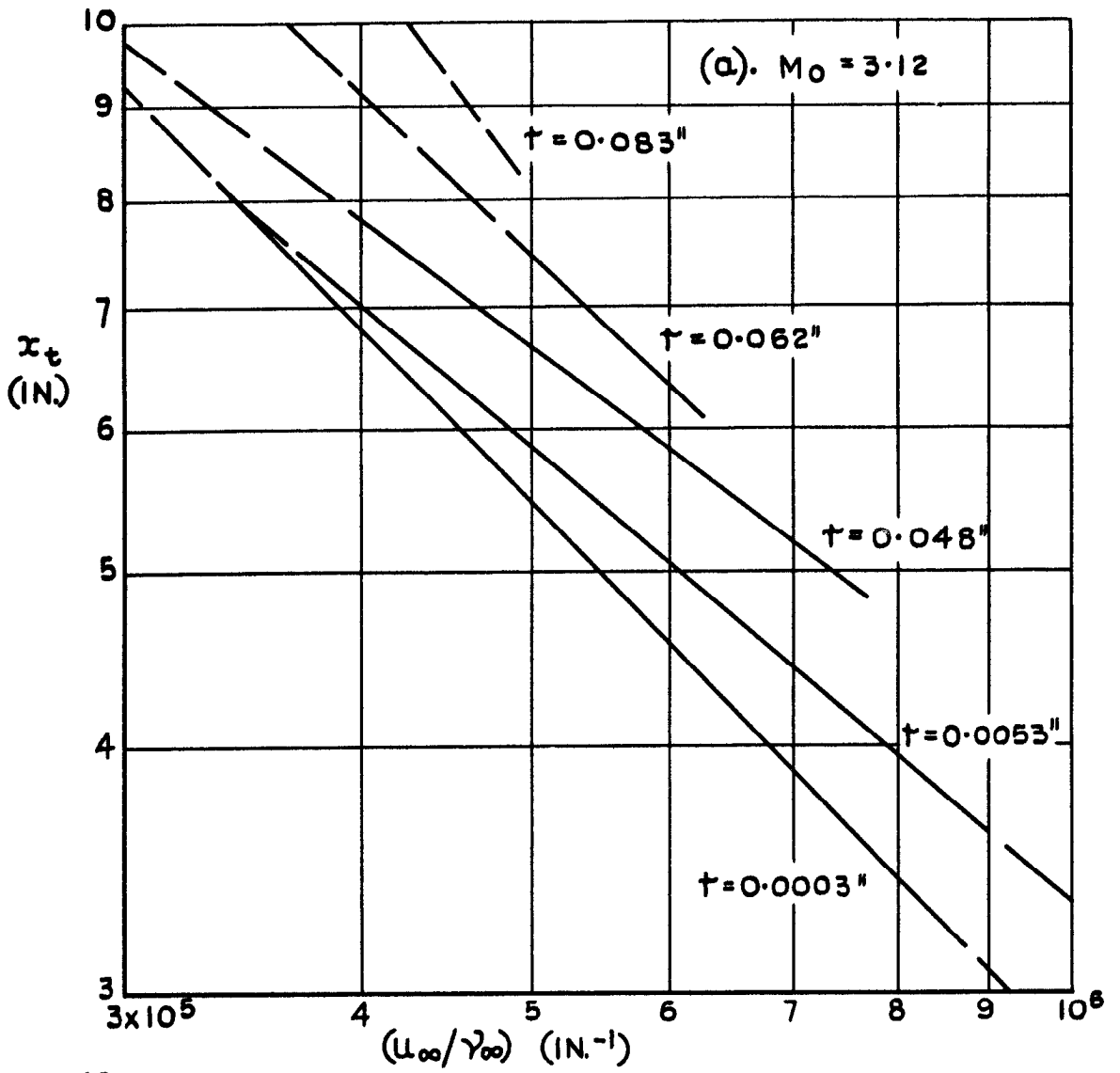

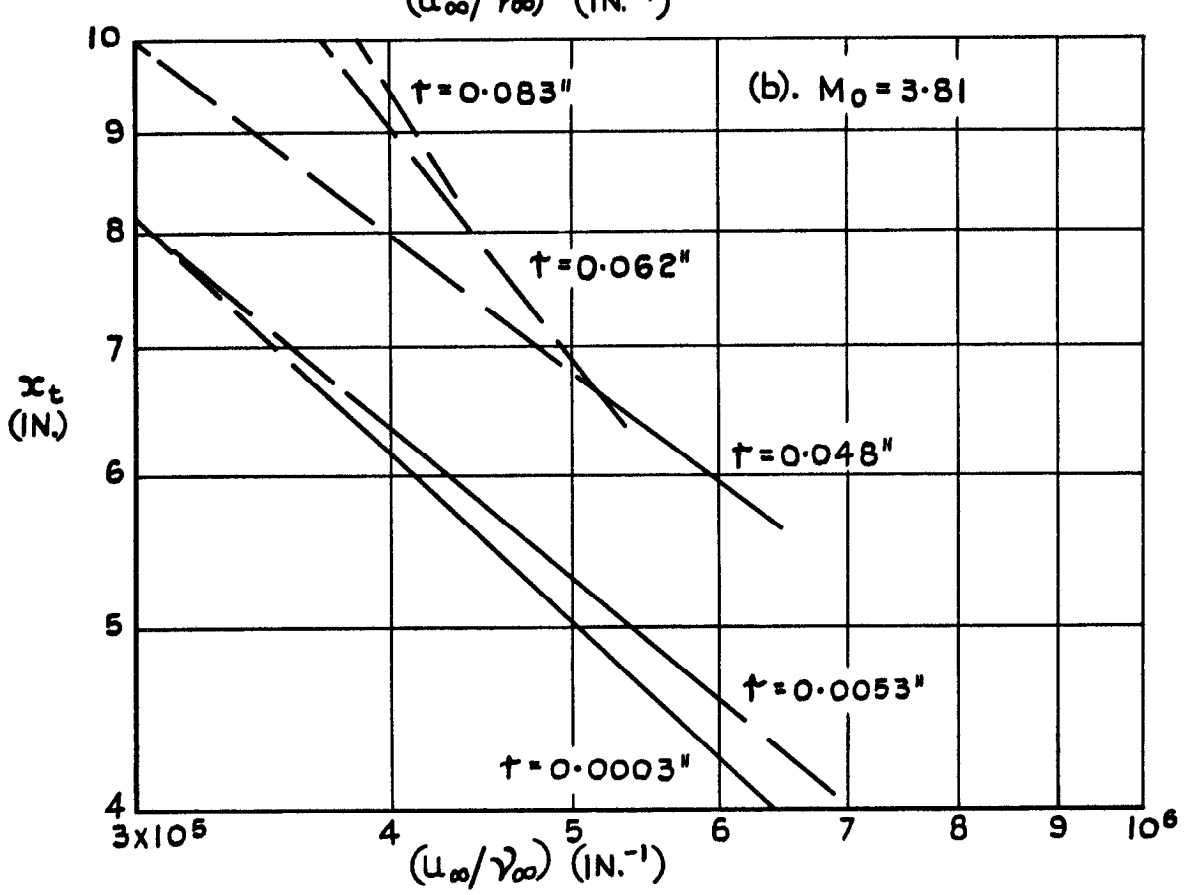

FIG.8. VARIATION OF TRANSITION POSITION, x_t, ON FIVE CONES WITH REYNOLDS NUMBER PER INCH, (u_0/ν_0), FOR $x_t > 100\,t$.
(CURVES FAIRED AND EXTRAPOLATED FROM MEASURED VALUES).
(a). $M_0 = 3{\cdot}12$, (b). $M_0 = 3{\cdot}81$.

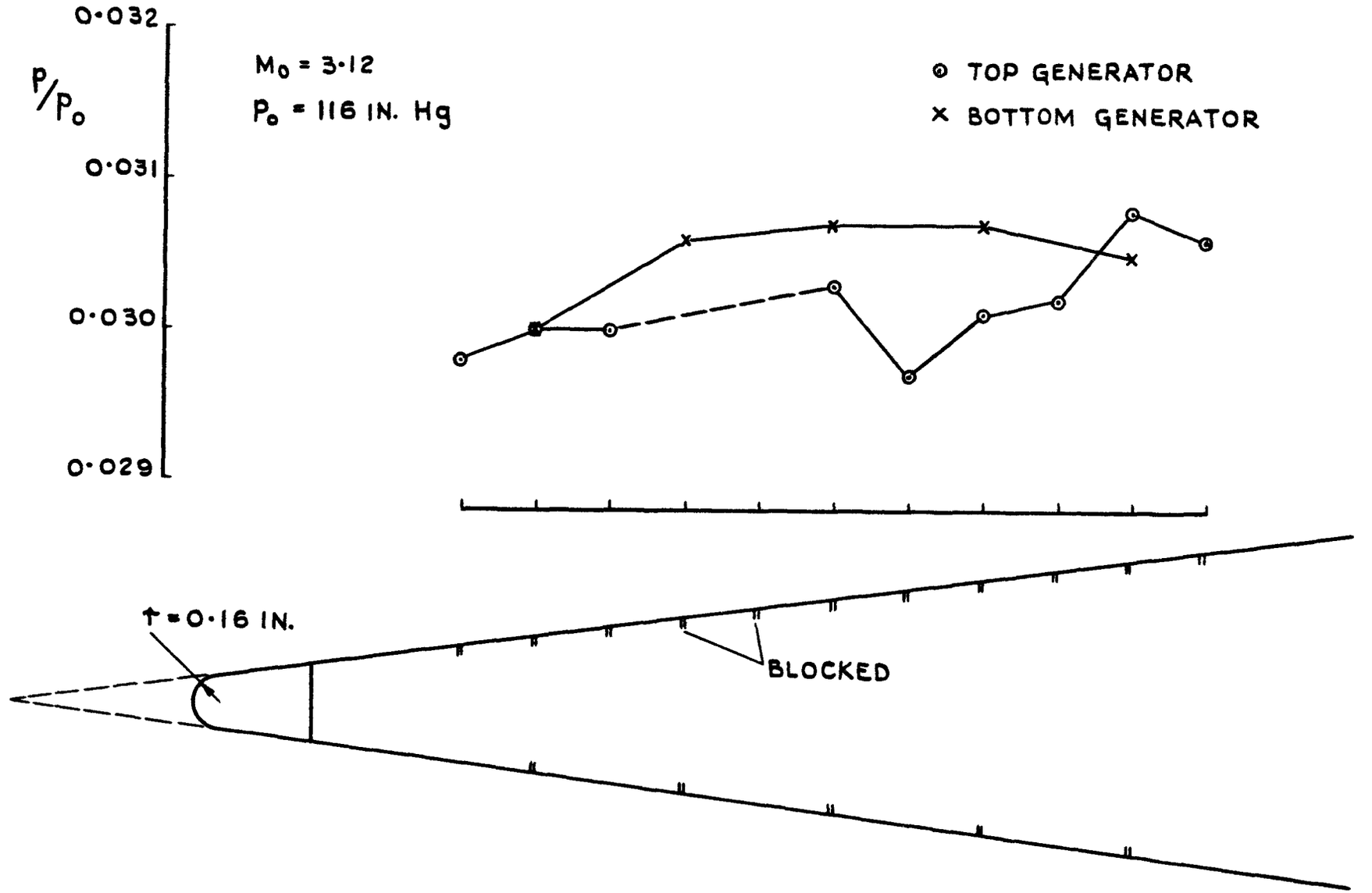

FIG.9. VARIATION OF STATIC PRESSURE ON THE SURFACE OF A BLUNT CONE WITH TIP RADIUS 0·16" ($M_0 = 3·12$).

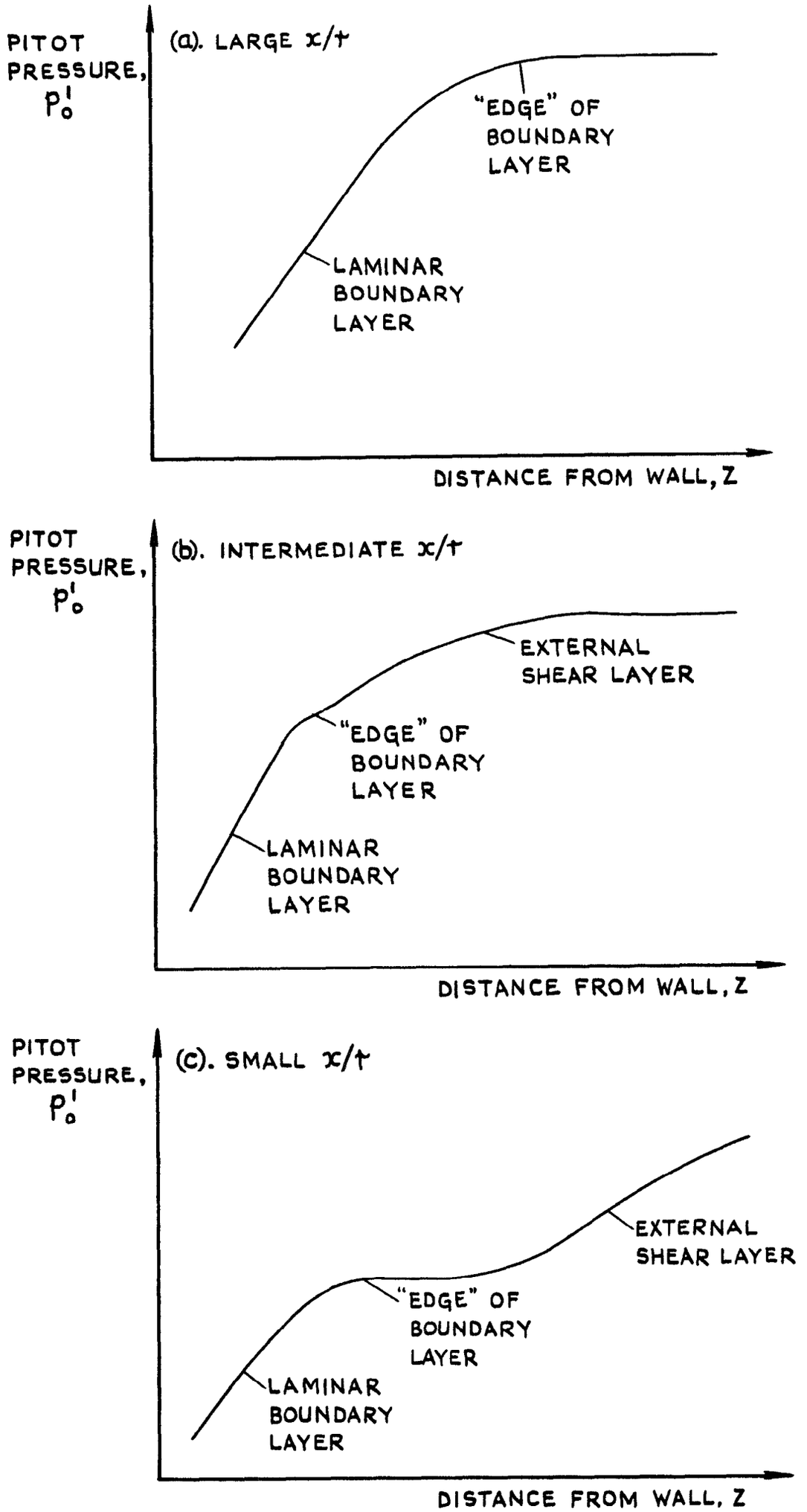

FIG.10. TYPICAL BOUNDARY-LAYER TRAVERSES AT DIFFERENT POSITIONS ON A BLUNT CONE. (NOT TO SCALE).

(a). LARGE x/r. (b). INTERMEDIATE x/r. (c). SMALL x/r.

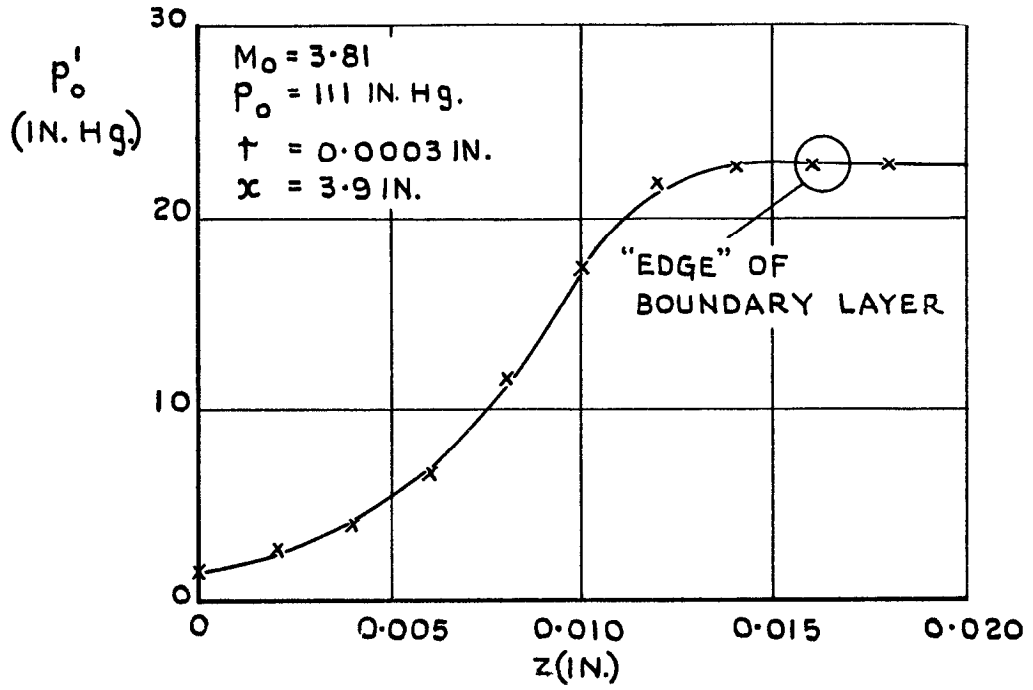

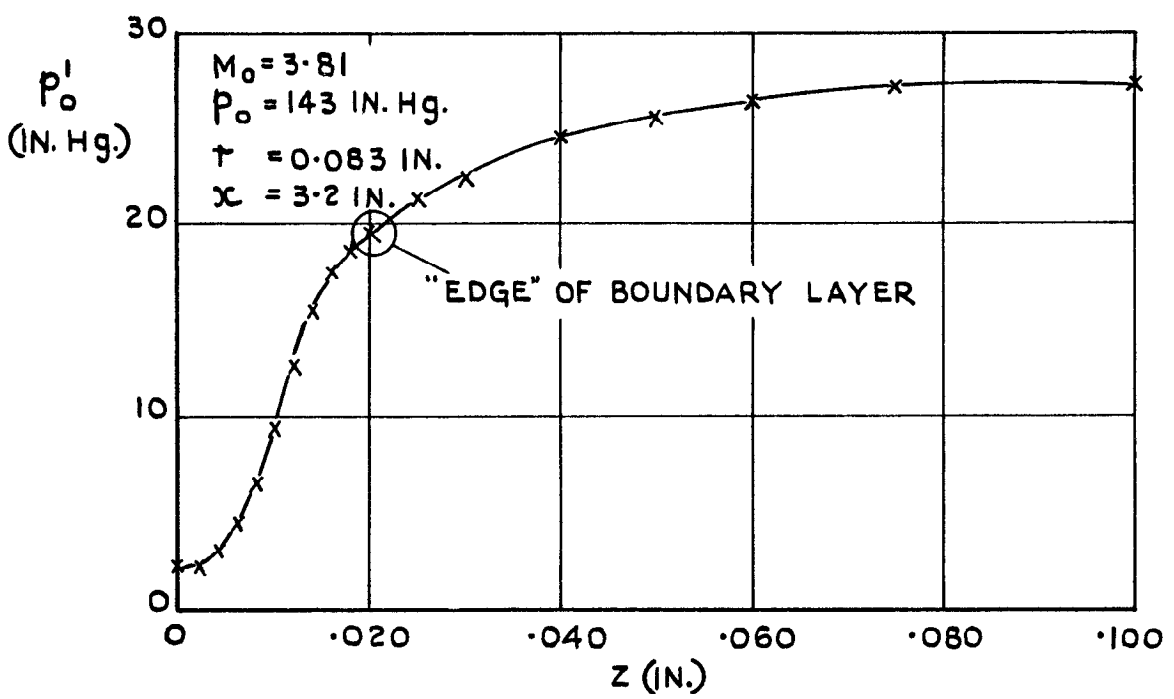

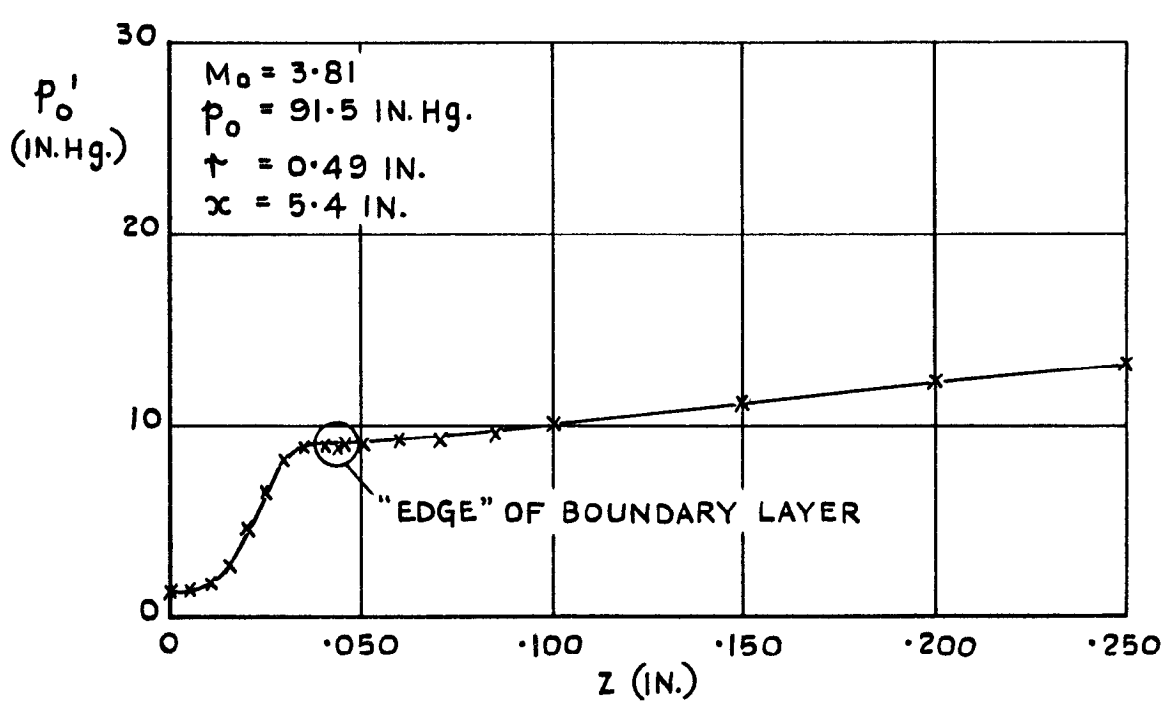

FIG.11. TYPICAL BOUNDARY-LAYER TRAVERSES.

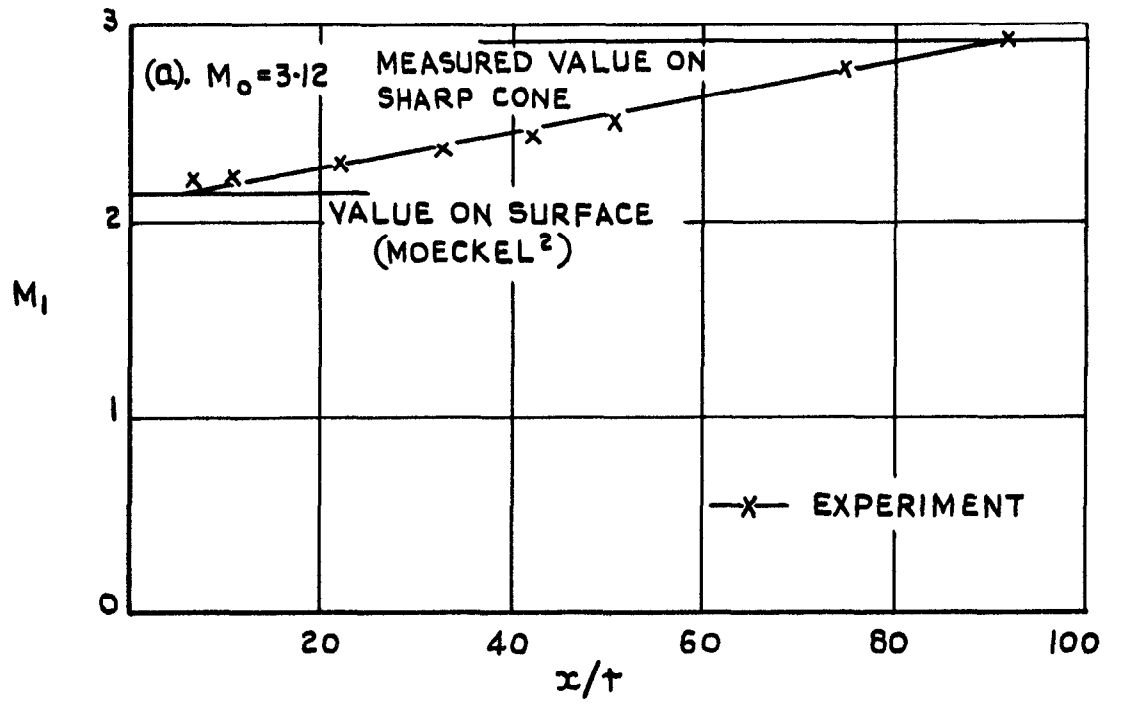

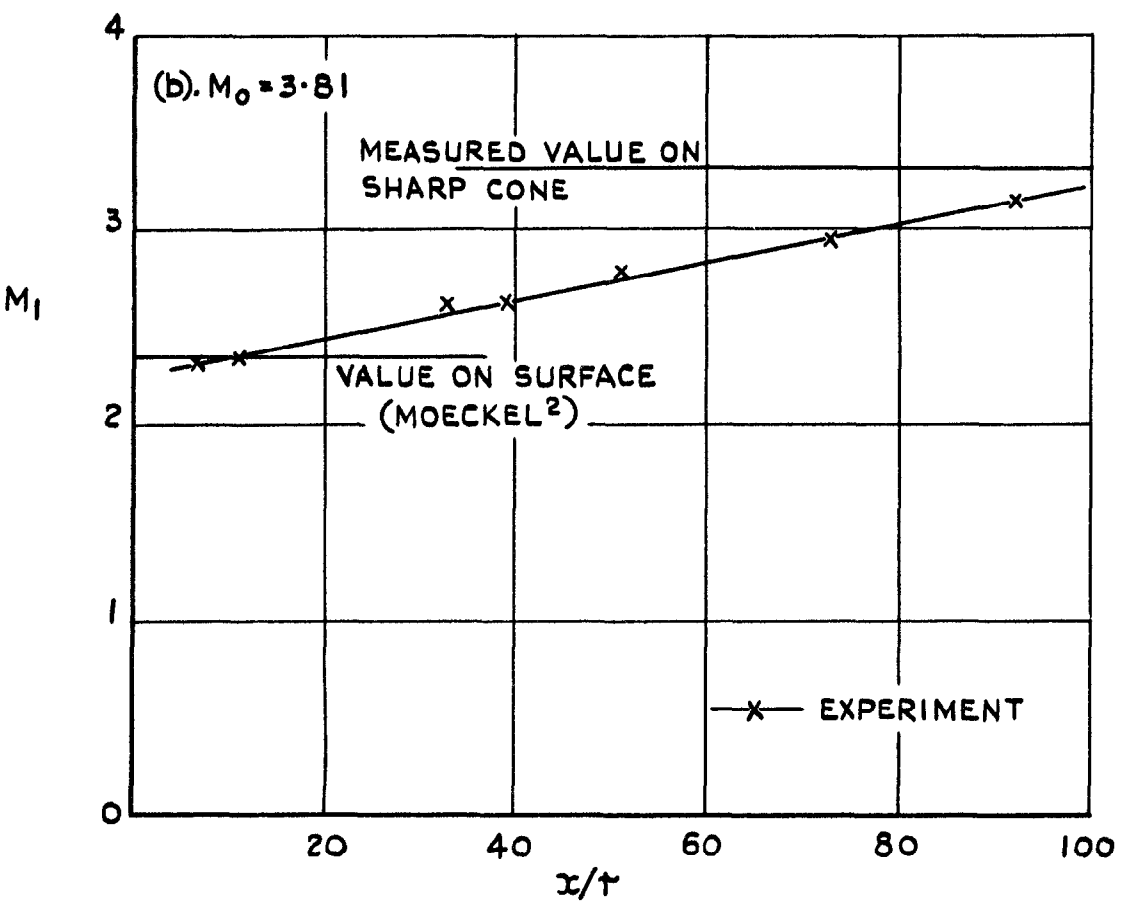

FIG.12. VARIATION WITH x/τ OF MEASURED MACH NUMBER AT EDGE OF LAMINAR BOUNDARY LAYERS ($x/\tau < 100$).
(a). $M_0 = 3{\cdot}12$, (b). $M_0 = 3{\cdot}81$.

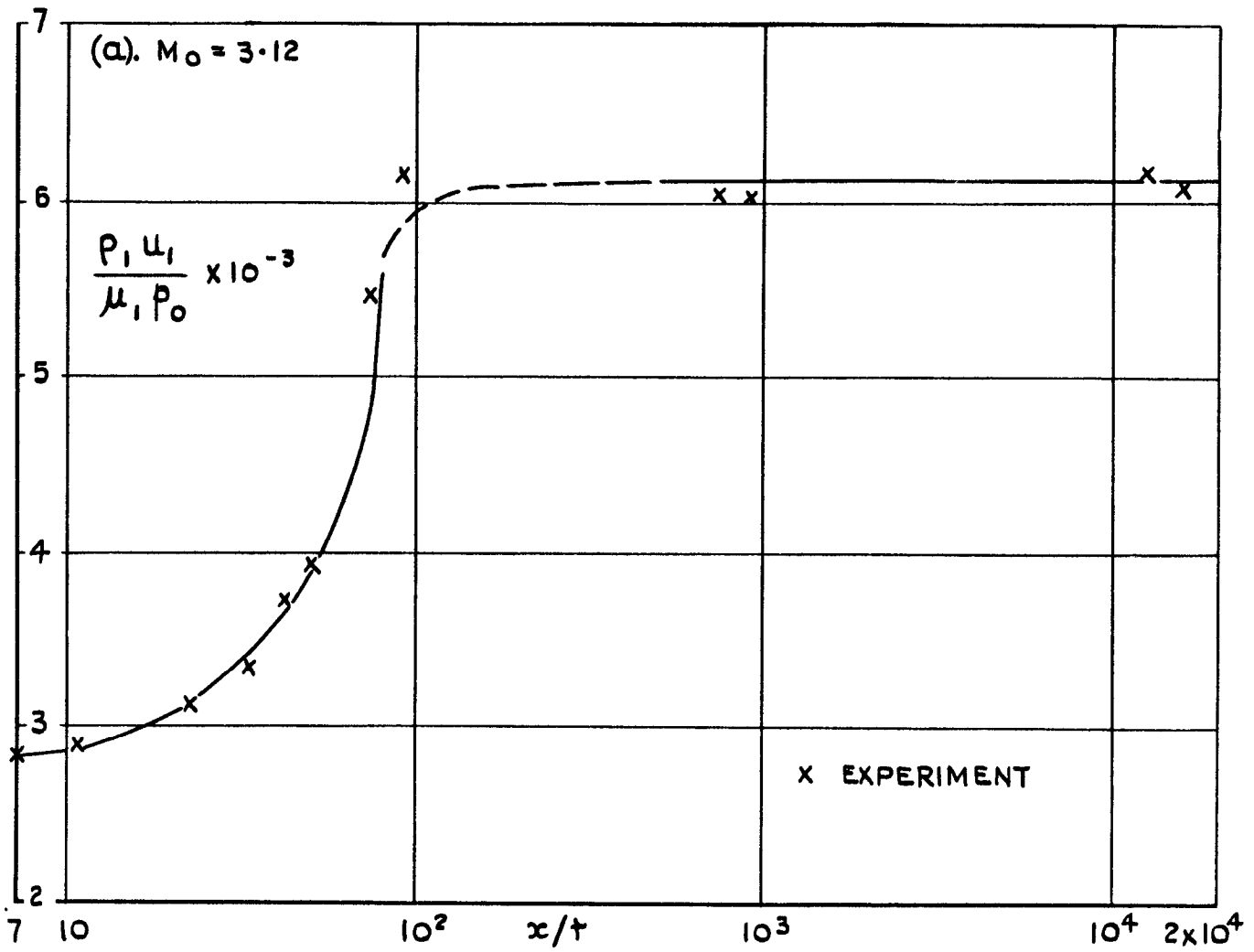

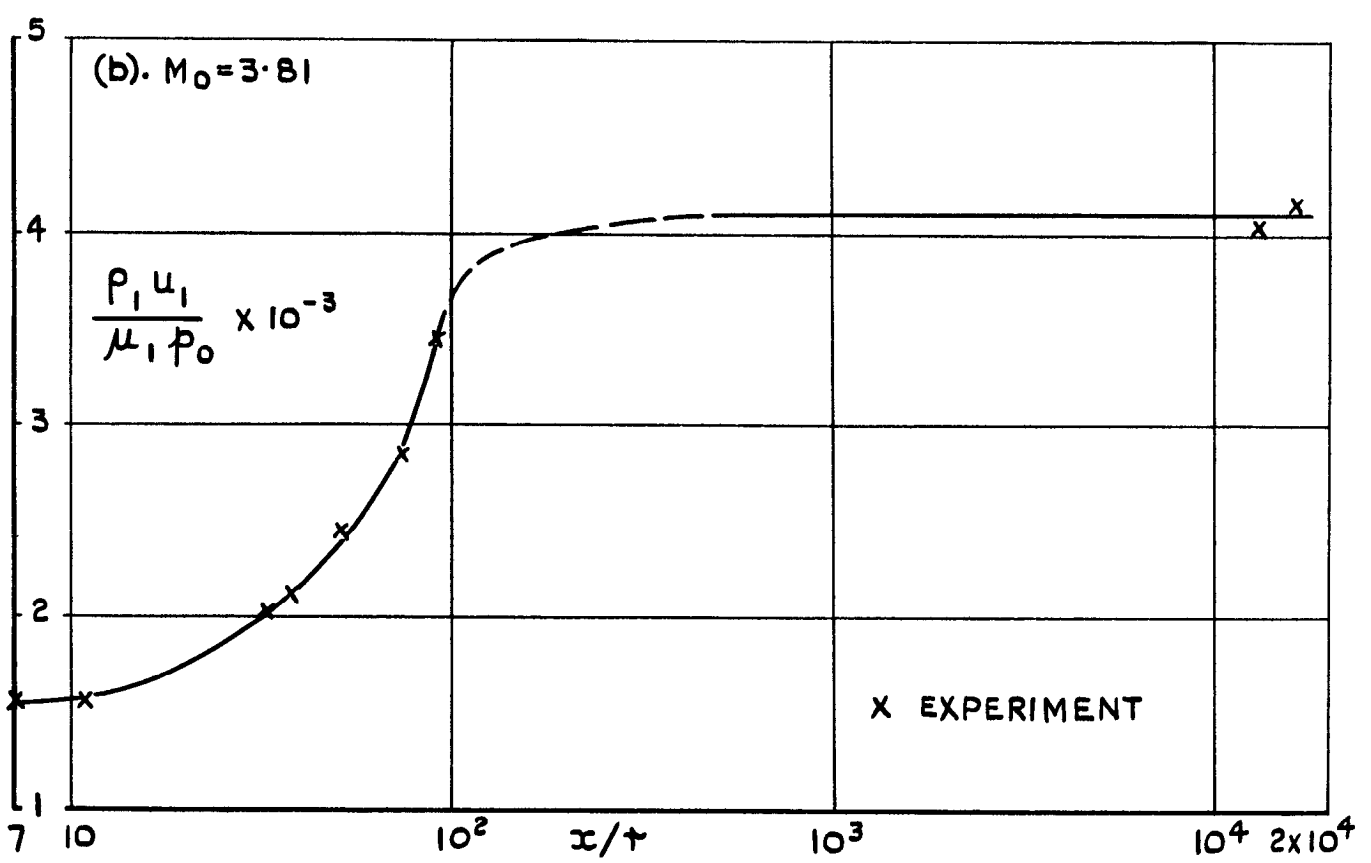

FIG.13. VARIATION OF $\rho_1 u_1 / \mu_1 \rho_0$ WITH x/t.
(a). $M_0 = 3{\cdot}12$, (b). $M_0 = 3{\cdot}81$.

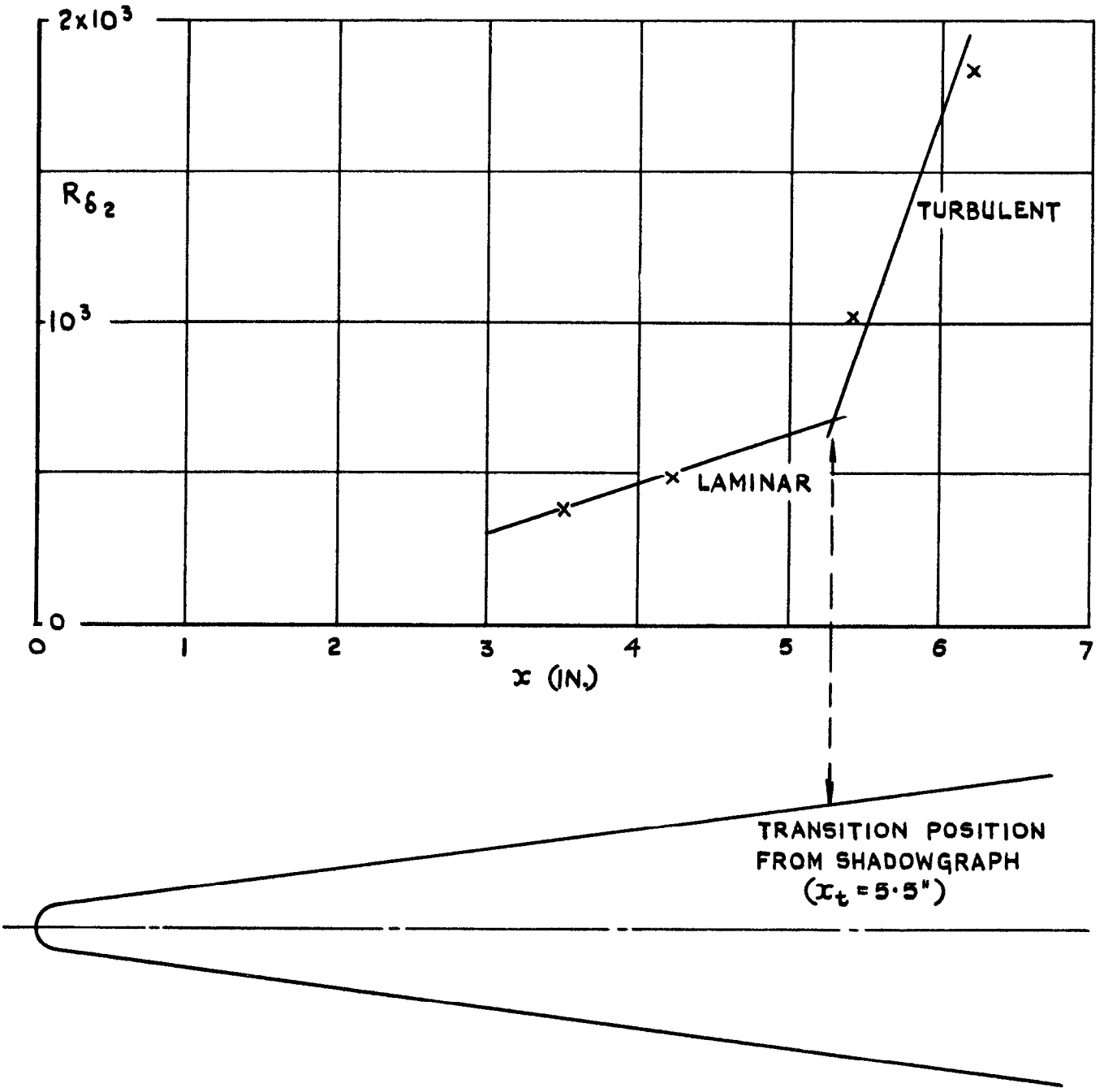

FIG.14. VARIATION OF LOCAL REYNOLDS NUMBER BASED ON MOMENTUM THICKNESS ALONG THE CONE WITH TIP RADIUS 0·083". (M_0 = 3·12).

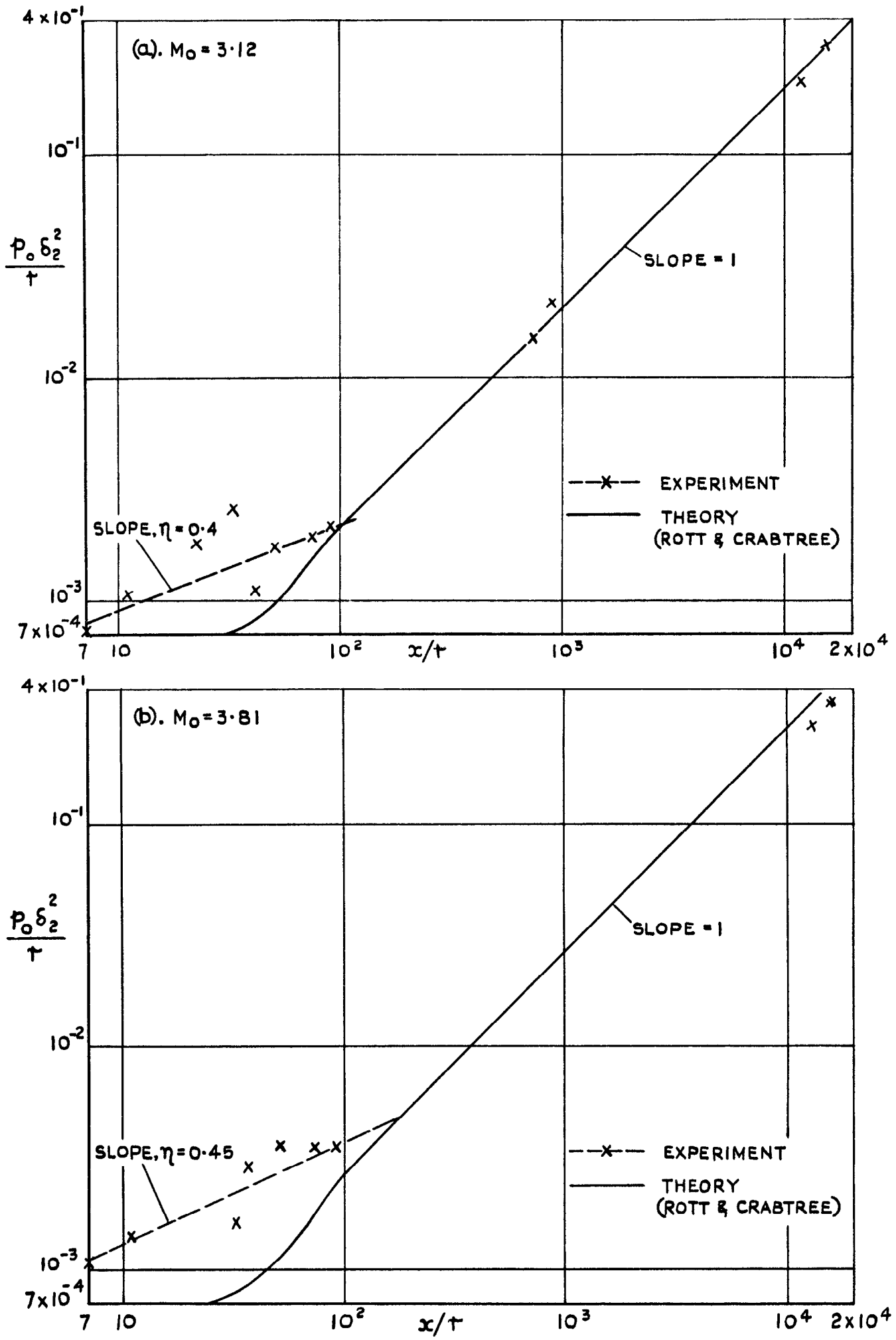

FIG.15. VARIATION OF $p_0\delta_2^2/t$ WITH x/t.
(a). $M_0 = 3{\cdot}12$, (b). $M_0 = 3{\cdot}81$.

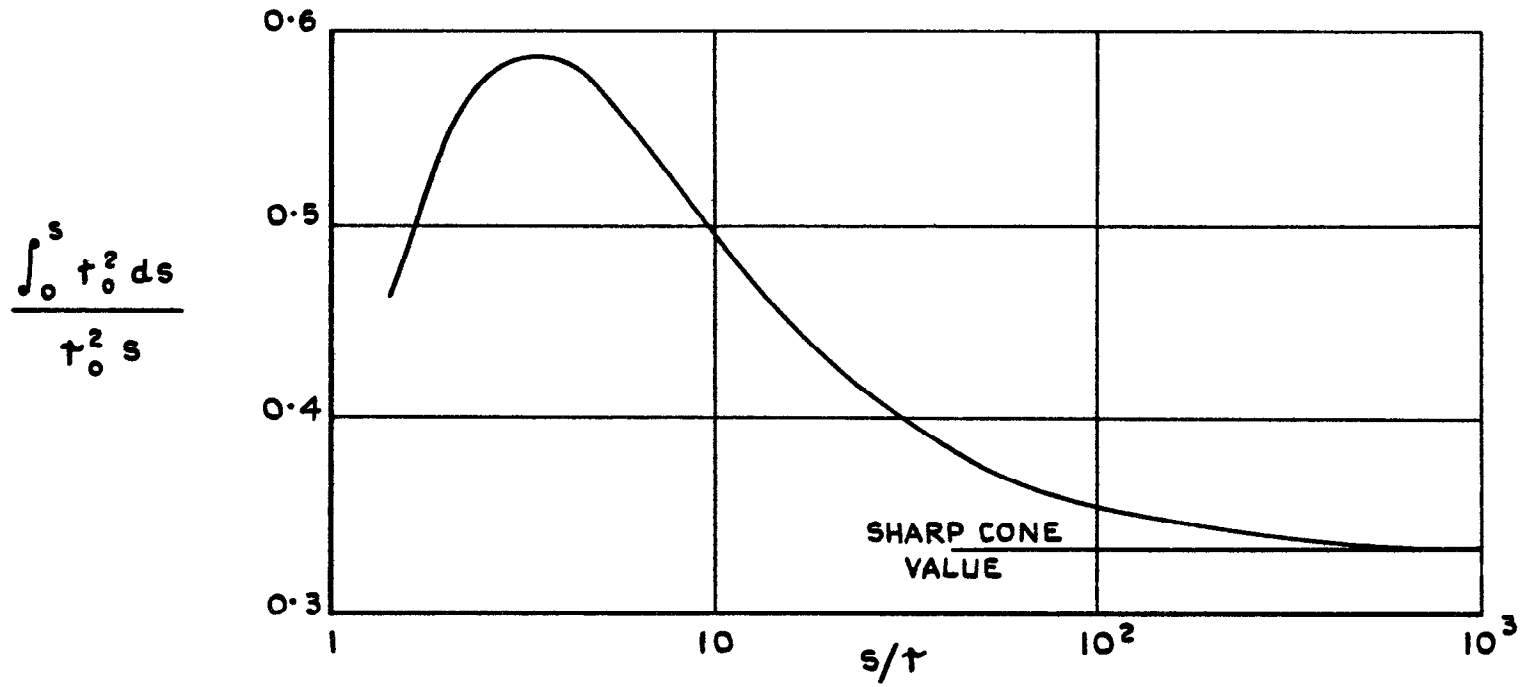

FIG.16. THE MANGLER TRANSFORMATION FOR A BLUNT 15° CONE.

at transition remained nearly constant in all cases (at 680 when M = 3.12 and 600 when M = 3.81). Some tentative arguments are put forward to explain the upstream movement of transition when occurring near the tip.

at transition remained nearly constant in all cases (at 680 when M = 3.12 and 600 when M = 3.81). Some tentative arguments are put forward to explain the upstream movement of transition when occurring near the tip.

at transition remained nearly constant in all cases (at 680 when M = 3.12 and 600 when M = 3.81). Some tentative arguments are put forward to explain the upstream movement of transition when occurring near the tip.

Published by
HER MAJESTY'S STATIONERY OFFICE

To be purchased from
York House, Kingsway, London W.C.2
423 Oxford Street, London W.1
13A Castle Street, Edinburgh 2
109 St. Mary Street, Cardiff
39 King Street, Manchester 2
50 Fairfax Street, Bristol 1
35 Smallbrook, Ringway, Birmingham 5
80 Chichester Street, Belfast 1
or through any bookseller

Printed in England

S.O. CODE No. 23-9012-98